Coversheet for “The Outflow Interactions Between Binary Tropical Cyclones”

Author 1: Lulabel Ruiz Seitz (lulabelseitz@gmail.com, Brown University)
Author 2: Laurel Régibeau-Rockett (regirock@stanford.edu, Stanford University)
Author 3: Ipshita Dey (ipshi91@stanford.edu, Stanford University)
Author 4: Morgan E O’Neill (morgan.e.oneill@gmail.com, Stanford University)

The Outflow Interactions Between Binary Tropical Cyclones

Lulabel Ruiz Seitz,[a b] Laurel Régibeau-Rockett,[c] Ipshita Dey,[c] Morgan E O'Neill[c]

[a] *Department of Applied Mathematics, Brown University, Providence, Rhode Island*

[b] *Department of Mathematics, Stanford University, Stanford, California*

[c] *Department of Earth System Science, Stanford University, Stanford, California*

Corresponding author: Lulabel Ruiz Seitz, lulabelseitz@gmail.com

ABSTRACT: The three-dimensional representation of an outflow jet can be used to assess whether interactions may have occurred between the outflows of binary, or spatially proximate, tropical cyclones, as outflow jets represent a dominant portion of the upper-tropospheric outflow for TCs. A novel algorithm, POJ3, for identifying and creating a three-dimensional representation of the principal outflow jet(s) of tropical cyclones is proposed. Validation of the algorithm is accomplished by comparing the output to previous findings that (1) the outflow jets of tropical cyclones preferentially form in regions of low potential vorticity and (2) outflow jets have a secondary circulation, which can be seen through signatures in relative humidity. We use POJ3 to investigate whether outflow interactions occurred between two pairs of binary tropical cyclones, Hurricanes Marco and Laura (2020) and Hurricanes Irma and Jose (2017). An examination of the three-dimensional jet locations together with the synoptic history, steering flow, and centroid-relative motion (or lack thereof) for the pairs of TCs indicates that Marco and Laura did not have significant outflow interactions whereas outflow interactions between Irma and Jose may be responsible for a significant diversion in Jose's track.

1. Introduction

A variety of interactions can occur between spatially proximate, also called binary, tropical cyclones (TCs), making forecasting their tracks and intensities more difficult (Dong and Neumann 1983; Lander and Holland 1993; Lander 1996; Prieto et al. 2003; Liu and Tan 2016). The Fujiwhara effect, in which two or more TCs rotate cyclonically about a centroid between their respective centers and ultimately merge, is the most well-known type of interaction between binary TCs (Fujiwhara 1921; Fujiwhara 1931). This phenomenon has been well studied and confirmed both observationally, in various cases of proximate TCs, and experimentally, through laboratory experiments and simulations using numerical models (Brand 1970; Dong and Neumann 1983; Lander and Holland 1993; Falkovich et al. 1995; Prieto et al. 2003). There has also been significant recent research on this topic (Liu and Tan 2016; De et al. 2022).

A complete merger as predicted by the classical Fujiwhara effect is not the only type of interaction between binary TCs that has been studied extensively. In fact, the classical Fujiwhara model is rarely observed. Instead, as the result of interaction between surface vortices, one TC may decay and be absorbed into a nearby "dominant" TC, involving "capture" and possibly "release" events (Lander and Holland 1993). The possible interactions between isolated vortices have been classified into five categories: elastic interaction, partial straining-out, complete straining-out, partial merger, and complete merger (Dritschel and Waugh 1992). The classical model has since been further modified to describe more general regimes of interaction: direct interaction, semidirect interaction, and indirect interaction (Carr et al. 1997). Direct interactions between TC vortices include one-way interactions, mutual interaction, and merger, which are all preceded by relative cyclonic motion of the TC centers. Semidirect interaction may at first appear to be direct interaction, as TCs undergo relative cyclonic motion, but is distinct in that track alteration is due to environmental flow rather than advection of one TC by the other TC's cyclonic circulation. Indirect interaction does not feature relative cyclonic motion, and describes the interaction between binary TCs and an anticyclone between them, which can form due to a Rossby wave train downstream of a large, leading TC. Indirect interactions have not been thoroughly studied; much remains to be understood about interactions between TCs that do not explicitly involve their surface vortices. Notably, the possibility of direct interactions between TC outflows has not been considered at all in these studies.

It is difficult to improve forecast capabilities in the case of binary TCs while the full set of their interactions remains poorly understood. In particular, how the trajectory of a storm's outflow may affect a downstream storm has not been studied, though this type of interaction would be relevant to more sets of binary TCs due to the further-reaching extent of TC outflow compared to the proximity necessary for the Fujiwhara effect. Moreover, despite this large body of work on the interactions between TC surface vortices, forecasting accuracy remains lower in the case of binary TCs (Liu and Tan 2016). Accordingly, determining whether the outflows of spatially proximate TCs can interact significantly may provide the necessary insight to eliminate the additional forecasting error when multiple TCs are present.

Given the recent increase of interest in the outflow layer and the consequent advances in research, it is an opportune time to investigate the potential for outflow interactions. This elevated focus on the outflow layer may be partially attributed to the development of modern remote-sensing-derived atmospheric motion vectors, which allow for better data collection at these levels (Ryglicki et al. 2019). Consequently, the Office of Naval Research Tropical Cyclone Intensity 2015 field campaign deployed over 800 dropsondes to gather precise observations of the outflow layers of Hurricanes Marty, Joaquin, and Patricia (Doyle et al. 2017). Besides advancements in the data available for the outflow layer of TCs, over the last few decades, the understanding of the outflow layer's role in modulating TC intensity has also developed significantly. By 1990, the general characteristics of tropical cyclone outflow layers were understood; observations revealed that they were typically anticyclonic, divergent, and asymmetric (Shi et al. 1990). Observations also showed that the outflow layer was dominated by one or two principal outflow jets (POJs), which are elongated, narrow regions of concentrated outflow. Using a three-dimensional idealized numerical model, Shi et al. (1990) confirmed these characteristics and observed a secondary circulation around the simulated outflow jet that left a distinct signature in relative humidity. In particular, the secondary circulation features an ascending branch near the center of the TC, a descending branch away from the center of the TC, an outward branch above the jet, and an inward branch below the jet. The Shi et al. (1990) study also found patterns in the potential vorticity (PV) around the outflow jet location; the tropopause defined by a surface of 0.2 PVU (2.0×10^{-7} m^2 s^{-1} K^{-1} kg^{-1}), was generally higher in terms of geometric height on the anticyclonic side of the jet and lower on the cyclonic side. The correlation between PV and the jet location has since been studied more extensively and has been theorized to be the result of a TC preferentially ventilating in a region of weak inertial stability, which in the absence of anomalously high static stability, corresponds to a region of negative or low PV (Rappin et al. 2011). Emanuel (2012) studied the role of entropy stratification in outflow and how it impacts tropical cyclone intensity, highlighting that the outflow layer is not a passive element in a storm, but an active one whose dynamics can impact the inner core and thus the storm's intensity. In light of this new understanding of the role of the outflow layer, studying outflow interactions may improve predictions of storm intensity and ultimately enhance the ability to mitigate the impacts of TCs.

As POJs represent a dominant aspect of a TC's outflow, identifying these jets is necessary in order to study realistic TC outflow. The only algorithmic method for identifying POJs, to our knowledge, involves selecting the streamline with nonnegative radial wind at a 500 km radius from the center with the maximum wind speed within a 1500 km radius of the center, at a characteristic outflow layer height (Merill 1988b). This simplified approach is not suitable in the case of proximate TCs, as increased wind speed near the center of one TC may bias the selected streamline for the other TC. If there are two TCs within 1500 km of each other, this approach may mistakenly identify any streamline emanating from the TC that goes towards the other TC, where it meets a region of higher wind speed, as the POJ. It also does not provide any information about how it varies in the vertical dimension. Other methods of identifying principal outflow jets have included analyzing isotachs, radial and tangential (or storm-relative meridional) wind components, and water vapor brightness temperature (Shi et al. 1990; Komaromi and Doyle 2017; Ditchek et al. 2017; Doyle et al. 2017). Like the approach in Merill (1988b), these also only yield a two-dimensional depiction of the outflow jet. These methods cannot yield a three-dimensional representation because they are not designed to take advantage of three-dimensional model output. An identification method specifically designed for three-dimensional model output will allow for usage of the numerous advantages of three-dimensional fields over two-dimensional simulated fields. Furthermore, these methods do not follow systemic approaches for identifying POJs, lacking objective criteria. Since it is vital to know the three-dimensional structure of the POJ when considering its interactions with another TC's outflow, and existing methods have significant limitations, we have developed a new methodology to identify POJs in order to study outflow interactions in a meaningful way.

We present a new algorithm, POJ3, that can identify these jets in numerical model data. Since a POJ is simply a channel of concentrated outflow that carries mass outside of the storm, we would expect it to be distinguished by a region of high mass flux travelling in the direction of the flow. While the locations of POJs do generally coincide with the region of highest wind speed near the storm, following mass flux instead helps to avoid anomalies that can come with considering wind speed alone, especially given that the streamlines can only be *approximated* from gridded wind data. The advantages of this method are firstly that the core jet region, or region of high mass flux, can be used to identify the vertical extent of the POJ, and secondly that it enables the POJ to deviate from any streamline approximating it. Having identified the POJ in forecast simulations, we support the validity of its identification by comparing the PV and relative humidity fields, and the three-dimensional structure of the jet, to what is expected based on prior work. The results of this comparison also suggest whether the algorithm's output could be easily approximated by distinctive signatures in these more readily calculated environmental fields. We find that while the identified POJ structure and locations do align with what is expected, they cannot be approximated in any comparable level of detail in this manner.

Using POJ3, Hurricanes Marco and Laura (2020) and Hurricanes Irma and Jose (2017) are used as case studies to illustrate ways in which the outflows between binary TCs can interact. Such characterizations may lead to a better understanding of when significant interactions between binary TCs can occur and how these interactions may impact the tracks or intensities of those TCs. There is potential for extending this methodology to explore the influence of different atmospheric systems on TCs through their interplay with TC outflow or vice versa.

The structure of the paper is as follows. In §2, the algorithm for identifying and creating three-dimensional representations of POJs is presented. The Python scripts required to run this algorithm and to visualize the output, as in this paper, are provided as supplementary files. In §3, the forecast simulation data from Hurricanes Marco and Laura and Hurricanes Irma and Jose, respectively, are used for preliminary outflow interaction case studies in order to illustrate the utility of POJ3. Synoptic information for each pair of TCs is provided, and observations about possible outflow interactions are discussed. Lastly, in §4, the results are summarized and directions for further work are discussed.

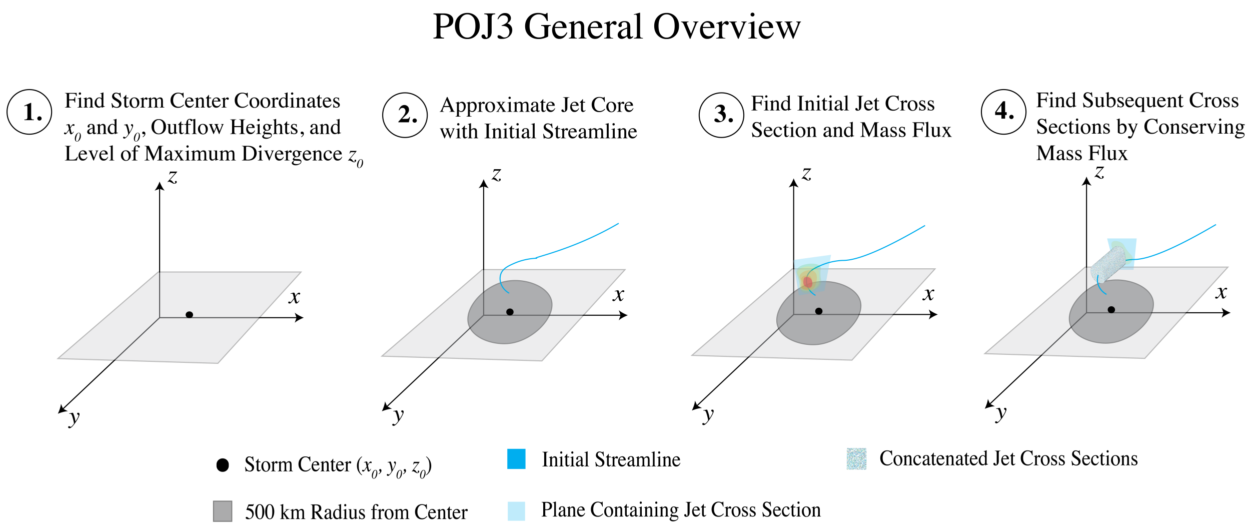

FIG. 1. POJ3's basic procedure follows four steps, as shown above. The $x-$ and $y-$ coordinates represent longitude and latitude, and the z coordinate represents descending pressure (or can be modified to be geometric height).

2. POJ3: Principal Outflow Jet Identification Algorithm

a. Overview

The general approach of POJ3 is as follows (Fig. 1). First, one must find the center location of the TC(s) at all relevant time steps, calculating the vertical extent of the outflow layer, and find the level of maximum divergence within the outflow layer. Then, the principal outflow jet or jets can be identified by successively finding cross sections that are normal to the dominant flow and that conserve mass flux.

To identify these cross sections, first, an initial streamline is identified, at either only the level of maximum divergence (the PROJECTED version of POJ3) or at all desired levels within the outflow layer (FULL version of POJ3). The initial streamline is the outgoing streamline with the maximum wind speed at 500 km from the storm center, that has not elsewhere entered the storm at 500 km. From there, the initial cross section of the jet is identified, and at every point along the initial streamline, a natural coordinate system is used to find a new cross section that conserves mass flux. A natural coordinate system is used in the sense that mass flux can only be computed across planes orthogonal to the flow, and the direction of the flow changes as the initial streamline is traversed geographically in the algorithm.[1]

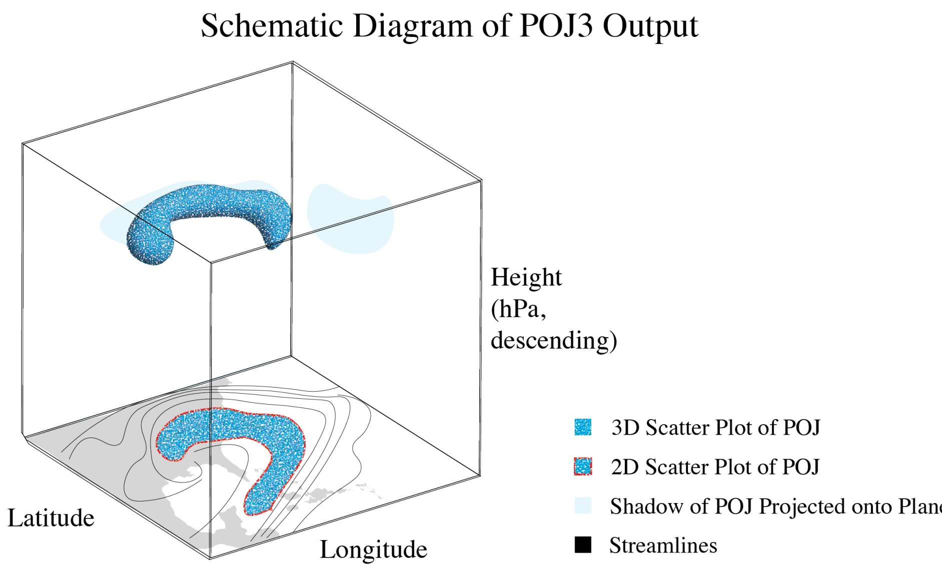

FIG. 2. Schematic diagram of the three-dimensional point-cloud output of POJ3, with a scatter plot projection onto the latitude-longitude plane with coastlines and streamlines drawn. The light blue solid regions correspond to projections of the three-dimensional jet onto each of the longitude-pressure and latitude-pressure planes.

Since any realistic jet is not expected to have an exactly cylindrical shape, it is necessary to *search* for the jet cross sections within the data rather than simply extrapolate from a center point. In other words, the definition of the POJ as a jet emanating from a wind speed maximum that conserves mass flux in orthogonal cross sections and follows the flow can also be described as a stream tube, the three-dimensional version of a streamline, for which there are existing formulas to determine the radius of any given cross section. Rather than using this idealized representation, we use a search procedure to approximate the sizes and locations of the orthogonal cross sections that conserve mass flux. The search space for these cross sections is limited prior to initiating the search, in order to limit computational cost. Concatenating the calculated jet cross sections together, POJ3 returns the coordinates of the jet in longitude-latitude-pressure space. These can be plotted in 2D (for a given pressure level) or 3D (all pressure levels) (Fig. 2).

[1]Note the difference between this instantaneous snapshot of the evolving flow, referred to as a streamline, and the technical definition of a streamline for a steady-state flow.

POJ3 is a series of Python scripts; scripts and documentation are provided in Supplementary Materials. POJ3 currently supports files from the Global Forecasting System (GFS), Hurricane Weather Research and Forecasting (HWRF), and Hurricanes in a Multi-scale Ocean-coupled Non-hydrostatic (HMON) models, which all output data in `.grib2` format with longitude, latitude, and pressure (hPa) coordinates.

b. Pre-Processing

Center location and outflow layer height data are required to run the algorithm.

1) Identifying TC Centers

The pressure centroid method for TC center identification has been found to yield more physically reasonable results than other methods (Nguyen et al. 2014). The version using geopotential height rather than pressure was used to accommodate the fact that the vertical coordinate for the model data that were used was pressure (hPa), and was only available in approximately 25 hPa increments for HMON and HWRF. For models where the coordinate is geometric or geopotential height, the original version is more readily employed. This method of determining the TC center involves iteratively making new guesses at the TC center, which is defined to be a centroid of geopotential heights at a constant pressure level, within a reasonable search domain, until one set of coordinates is converged upon. The constant pressure level at which the geopotential heights of the various points were considered was 800 hPa, rather than surface level, in order to avoid the influence of topography. The initial guess of center coordinates (x_0, y_0), where x_0 is longitude (degrees east) and y_0 is latitude, is the location of minimum geopotential height in the approximate region where the storm is located at a given time step. Then, new guesses of coordinates x_i, y_i are calculated by

$$x_i = \frac{\sum_{r=0}^{250} \sum_j x_{rj} GH'_{rj}}{\sum_{r=0}^{250} \sum_j GH'_{rj}}, \quad y_i = \frac{\sum_{r=0}^{250} \sum_j y_{rj} GH'_{rj}}{\sum_{r=0}^{250} \sum_j GH'_{rj}}$$

where j is the index running over all points at a given radius r (km) from the previous guess, starting with the initial guess (x_0, y_0), and

$$GH'_{rj} = GH_{env} - GH_{rj},$$

where GH_{env}, or the environmental geopotential height, is the average geopotential height along a 500 km radius centered at the previous guess (x_{i-1}, y_{i-1}), and GH_{rj} is the geopotential height of the point at radius r with index j. Thus, each new guess (x_i, y_i) is calculated by weighting each grid point within a 250 km radius of the previous guess by its differential geopotential height GH'_{rj}, eventually yielding a stationary pair of coordinates representing the center point.

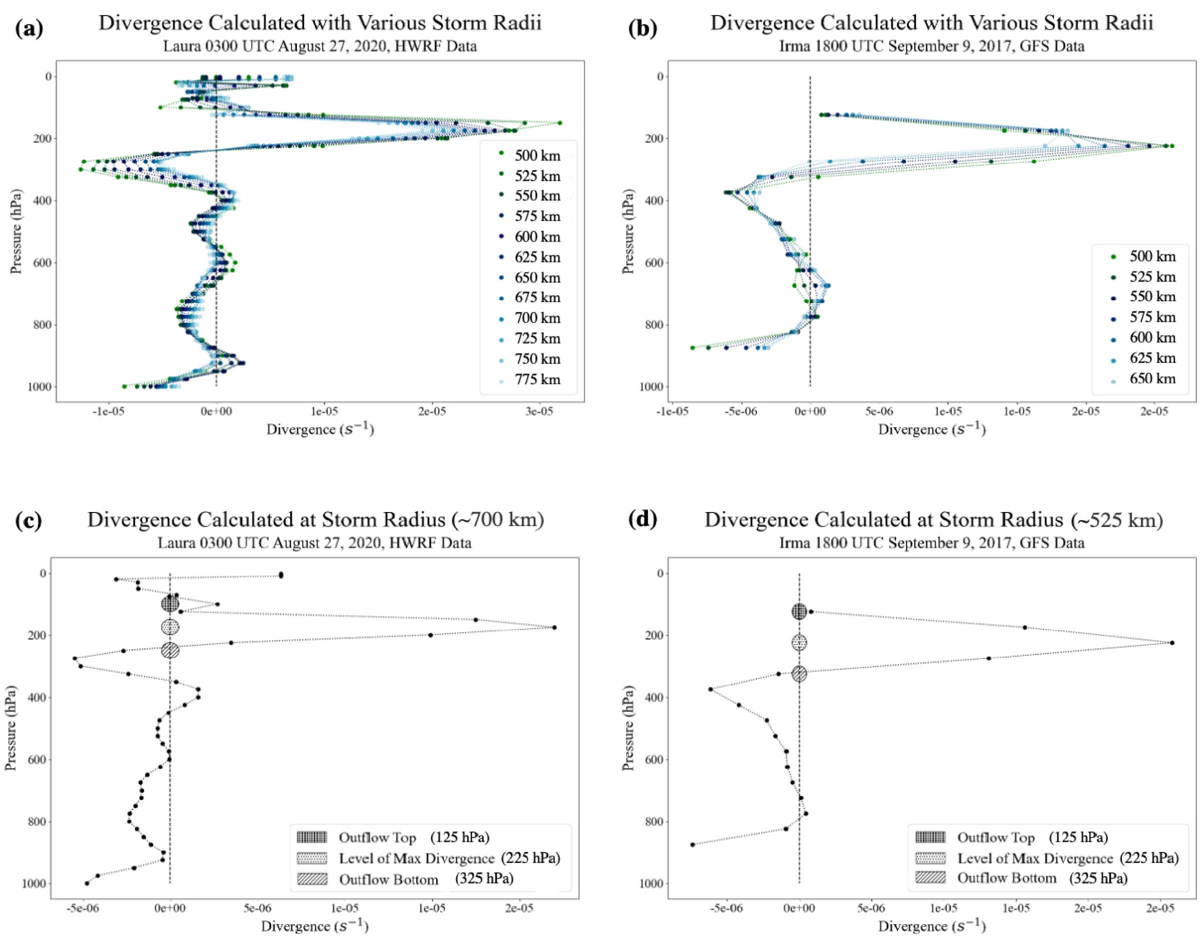

FIG. 3. **(a)** Divergence calculated for various possible storm radii, ranging from 500 km to 775 km for Laura (HWRF, initialized 0000 UTC August 27, 2020, valid time 0300 UTC August 27, 2020, 0.25 degree horizontal spacing, 25 hPa vertical spacing). **(c)** Divergence calculated for computed storm radius of 700 km for Laura (same data), with outflow top, outflow bottom, and level of maximum divergence values labelled. Figures **(b)** and **(d)** are the same as **(a)** and **(c)** but for Irma (GFS, initialized 1200 UTC September 9, 2017, 1800 UTC valid time September 9, 2017, 0.25 degree horizontal spacing, 50 hPa vertical spacing.)

2) Location of the Outflow Layer

To find the vertical extent of the outflow layer, at each height (in hPa) for which data were available, the area-weighted divergence was calculated within an approximate storm radius from the center. The storm radius was defined to be the radius at which the surface-level azimuthal-mean azimuthal wind is 12 m s^{-1} (Chavas et al. 2015). To approximate the surface wind but account for the impact of topography, data at the 850hPa level were used. The outflow layer is typically found between 300 hPa and 100 hPa (Merrill and Velden 1996). Accordingly, the bottom of the outflow layer was defined to be the level nearest to 300 hPa at which the TC transitioned from exhibiting convergence to divergence, or a local minimum in divergence. The top of the outflow layer was defined to be the level nearest to 100 hPa at which the TC transitioned from exhibiting divergence to convergence. Notably, as shown in Fig. 3, the lower and upper bounds of the outflow layer defined this way were almost independent of the radius size chosen. The level of maximum divergence was also found using the area-weighted divergence within the storm radius (Fig. 3).

c. Algorithm

POJ3 can be used to search for one jet or two jets, and has both a plane-view version (PROJECTED) and a more comprehensive version (FULL). The PROJECTED version estimates the flow at all relevant outflow levels by projecting the line normal to the flow at the level of maximum divergence onto the other levels. In contrast, the FULL version calculates a line normal to the flow at each relevant outflow level. In the following section, the steps associated with each of the four versions is discussed, which is also shown in Fig. 4.

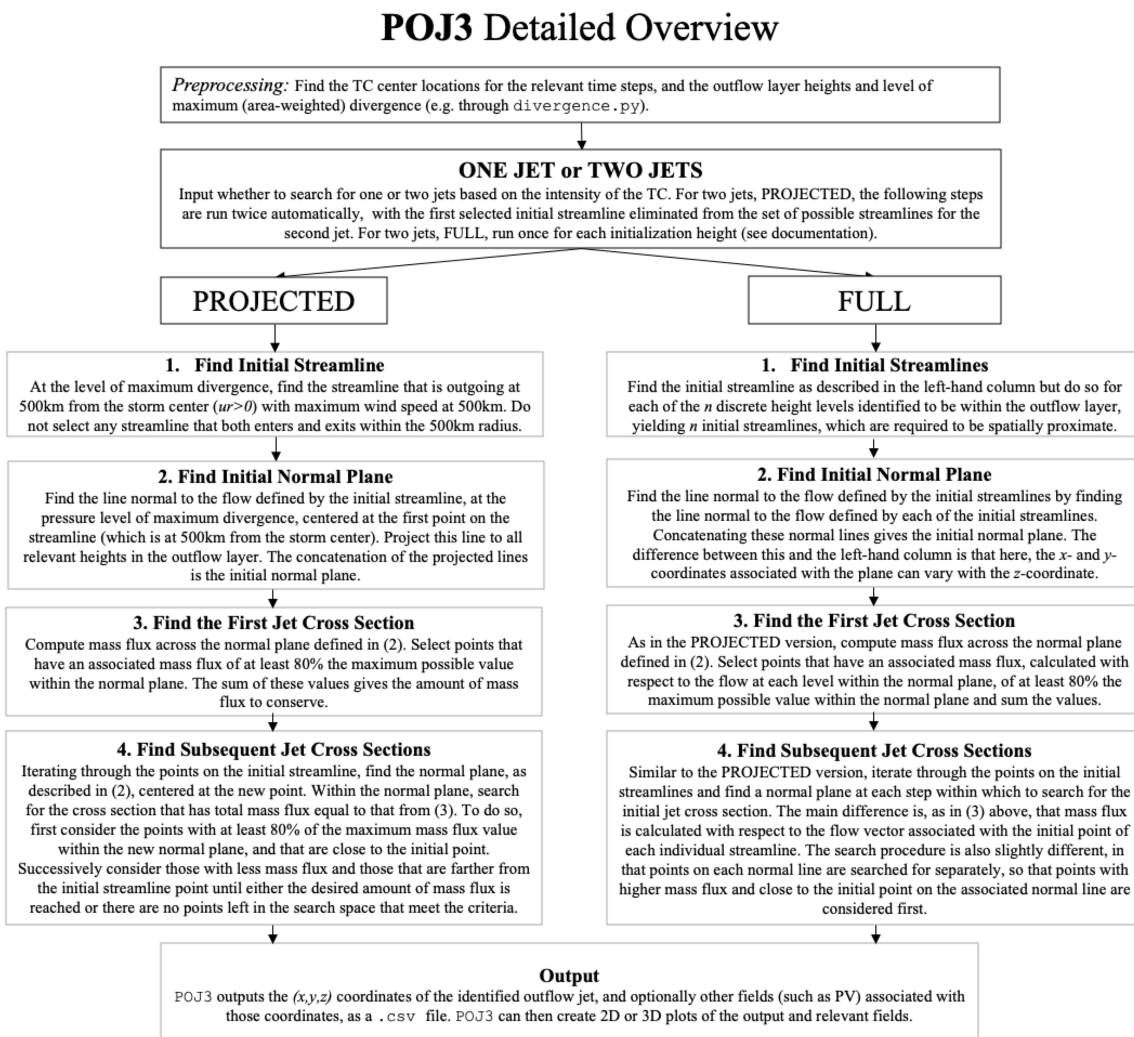

Fig. 4. A full overview of POJ3, including the specifications for all modes of the algorithm.

1) One Jet

1. Initial Streamline

After loading the data, finding the center location for the TC, the vertical extent of the outflow layer, and the level in the outflow layer at which there is the maximum amount of divergence, POJ3 determines initial streamline(s) on which to center the search space for the jet cross sections. If the PROJECTION option is selected, POJ3 determines *one* initial streamline at the level of maximum divergence within the outflow layer and projects that to all other relevant levels. If the FULL option is selected, POJ3 determines an initial streamline at *every* desired level within the outflow layer that is sufficiently close horizontally to the initial streamline at the level of maximum divergence. To find the initial streamline at a given level, first, all the streamlines within a limited domain about the storm center are computed.[2] Then, of the streamlines with positive radial wind that exit and do not re-enter the storm within a 500 km radius, the streamline that has the maximum wind speed at 500 km is chosen as the initial streamline. The 500 km value is somewhat arbitrary, but has been used as a threshold for where outflow begins, both in the previous algorithm and otherwise (Merrill 1988a; Komaromi and Doyle 2017). The wind speed at 500 km rather than past that threshold is considered to avoid the influence of other features in the environment that are associated with high wind speeds. An example of the candidate and chosen streamlines, as well as those that were disqualified for re-entering the storm before exiting, are shown in Fig. 5.

2. Initial Cross Section

The initial mass flux cross section is then determined. However, as mass flux is computed through a plane orthogonal to the flow, POJ3 first identifies such a plane, centered at the first longitude, latitude point (ψ_0, ϕ_0), on the initial streamline. This plane is centered 500 km from the storm center and is defined using the horizontal wind vectors associated with a given point in the streamline. Note that we do not consider the vertical "tilt" of the normal plane, because horizontal motion is dominant in the POJ, with the vertical wind component typically at least an order of magnitude less than the horizontal components. Additionally, due to the coarseness of the vertical coordinate (pressure), allowing the normal plane to tilt based on the vertical velocity would cause little to no variation in the defined plane.

[2]Computing the streamlines is the most computationally expensive part of the algorithm. By limiting the domain, the computational cost may be decreased: see documentation.

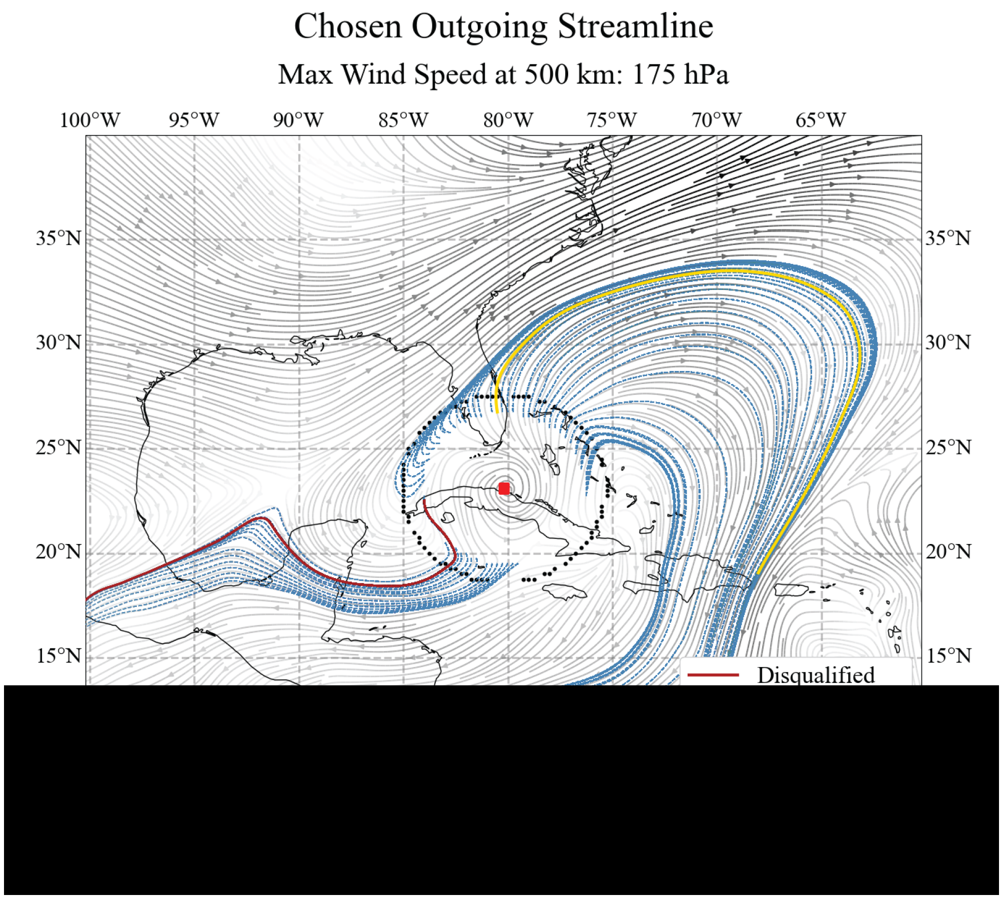

[redacted]

FIG. 5. Example of the chosen outgoing streamline (yellow) for Irma (GFS, initialized 1200 UTC September 9, 2017 1200 UTC, valid time 1800 UTC September 9, 2017, 0.25 degree horizontal grid spacing, 50 hPa vertical grid spacing) at a pressure level of 175 hPa among all candidate streamlines (dashed, blue) as well as a streamline that was disqualified (red) for crossing a radius within a 500 km storm radius (black dots) at multiple points. The storm center is also shown (red square). All streamlines in the domain at 175 hPa are shown in the background, shaded by wind speed (darker is higher wind speed).

A normal vector $\vec{n} = (-v, u)$ is defined using the components of the horizontal wind, i.e. the tangent vector at a point along the streamline. This yields a line normal to the flow at this point, which has tangent vector $\vec{v} = (u, v)$, since

$$\vec{v} \cdot \vec{n} = -uv + vu = 0.$$

This normal line is found across an approximately 2.5 degree longitude by 2.5 degree latitude box, to allow reasonable but not excessive deviation from the initial streamline. It is defined by all j points with latitude, longitude coordinates (ψ_j, ϕ_j) that create the same angle with (ψ_0, ϕ_0) as does the vector $\vec{n}$, i.e. such that

$$\arctan\left(\frac{\phi_j - \phi_0}{(\psi_j - \psi_0)\cos(\phi_j)}\right) = \arctan\left(\frac{u}{-v}\right).$$

The cosine in the denominator accounts for the fact that the horizontal distance between the longitudes differs based on the corresponding latitude. Since arctan is bijective, we can compute this by simply comparing the ratios (i.e., by left-composing with $\arctan^{-1}$). However, the resolution is too sparse to find exactly a line of points, so POJ3 finds a patch of points.

In test cases, the search space was large enough to encapsulate jet cross sections even if they were not perfectly centered on the initial streamline. However, if the search space defined by the projection of the identified normal line to all pressure levels is somehow not large enough to encapsulate the jet cross section, the FULL version may be run as it allows for more variation, i.e. the jet to "swerve" more. When the FULL version of the algorithm is selected, a streamline with flow vectors is found for each relevant pressure level, and so a different normal line is computed for each pressure level rather than projecting the flow at the level of maximum divergence onto the others. In both versions, the jet cross section is then a subset of the plane formed from the normal lines at each relevant pressure level. While we will refer to the set of points forming a cross section of the jet as a "plane" throughout this paper, in the case of the FULL version of the algorithm, it may be "curved" – i.e. x and y may vary nonlinearly with z – and it thus may be more generally a surface rather than a plane.

From there, all points within that plane meeting or exceeding a certain mass flux threshold are identified as the jet (Fig. 6). In this work, all points that have an associated mass flux of at least 80% of that of the maximum within the normal plane are selected as the initial jet cross section. The 80% value was empirically and subjectively determined to correspond to the contour of concentrated mass flux in various test cases, as there is no threshold defined for the relative concentration of the flow *a priori*. However, this threshold value may be increased or decreased by the user as a parameter to yield a narrower or wider jet, respectively, as described in the POJ3 documentation. Additionally, the jet region identified is insensitive to single order of magnitude changes to this threshold, but more variance in the jet location results from higher order changes of magnitude.

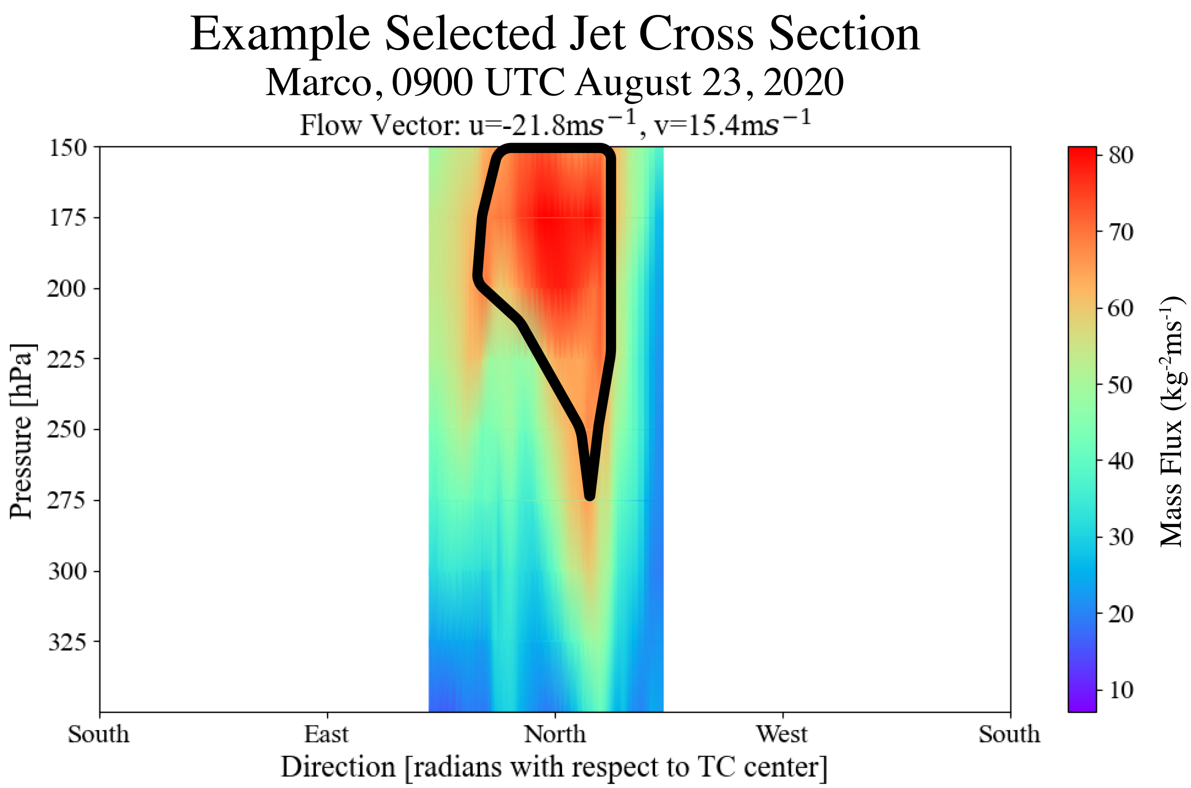

FIG. 6. A jet cross section for Hurricane Marco (HWRF, initialized 0600 UTC August 23, 2020, valid time 0900 UTC August 23, 2020, 0.25 degree horizontal grid spacing, 25 hPa vertical grid spacing), as seen by the concentrated contour of mass flux in orange/red. The thick black line surrounds the approximate initial jet cross-section. In this case, the black line surrounds the points within the normal plane which have associated mass flux values at least 80% of that of the maximum. Note that Gouraud shading was used, and due to the gridded data, is only approximate.

Mass flux (assuming a constant time increment Δt) of a fluid with density ρ at a point $p = (\phi_j, \psi_j, \xi_j)$ across a plane orthogonal to the flow is given by

$$\rho \vec{v} \cdot \hat{n}$$

where $\vec{v} = (u_v, v_v, w_v)$ is the three-dimensional flow vector at a point p in the plane and $\hat{n}$ is a unit normal vector to that plane. In our case, the plane of consideration is defined to be normal to the tangent vector associated with the point along the initial streamline, $\vec{r} = (u_t, v_t, w_t)$, i.e. $\hat{n} = \hat{r}$, where $\hat{r}$ is the unit tangent vector. This is equivalent to considering the coordinate rotation that would be involved in forming a natural coordinate system according to the flow, i.e.

$$\rho||\vec{v}||\cos(\theta)$$

where θ is the angle between the flow vector at p and the normal plane. While these calculations give us the mass flux associated with a particular point, we are using gridded data, so we must take each point to be representative of its surrounding space in the grid. Accordingly, we could multiply this value by the difference between geometric heights of the levels, approximating all vertical layers for which there are no data as having the same data as the layer below. Recall that the plane defined above by the normal line (PROJECTED) or lines (FULL) is approximately orthogonal, since the vertical component of the flow is negligible for this calculation. Thus, the mass flux calculation is valid on this region. Then, for one height level, taking that level to be representative of all dz of height above or below it, the mass flux in units of kg m^{-2} s^{-1} is given by

$$\rho(\vec{v} \cdot \hat{r})dz.$$

Applying hydrostatic balance, this can also be computed as

$$-(1/g)(\vec{v} \cdot \hat{r})dP.$$

Summing up this value for every point within the isobaric layer, over all relevant vertical layers that have at least a contiguous point exceeding the mass flux threshold, would give an estimation of the total mass flux represented by this region. Note that the magnitude of the constant scalar quantities does not matter because only the relative and not the absolute magnitudes of mass flux will be compared in order to choose points for the jet. This is also why the horizontal distances between adjacent points are approximated as equal and scaled to one for the sake of computational efficiency. Only the normalization of $\vec{r}$ is actually necessary for comparing different jet regions if the grid spacing is the same.

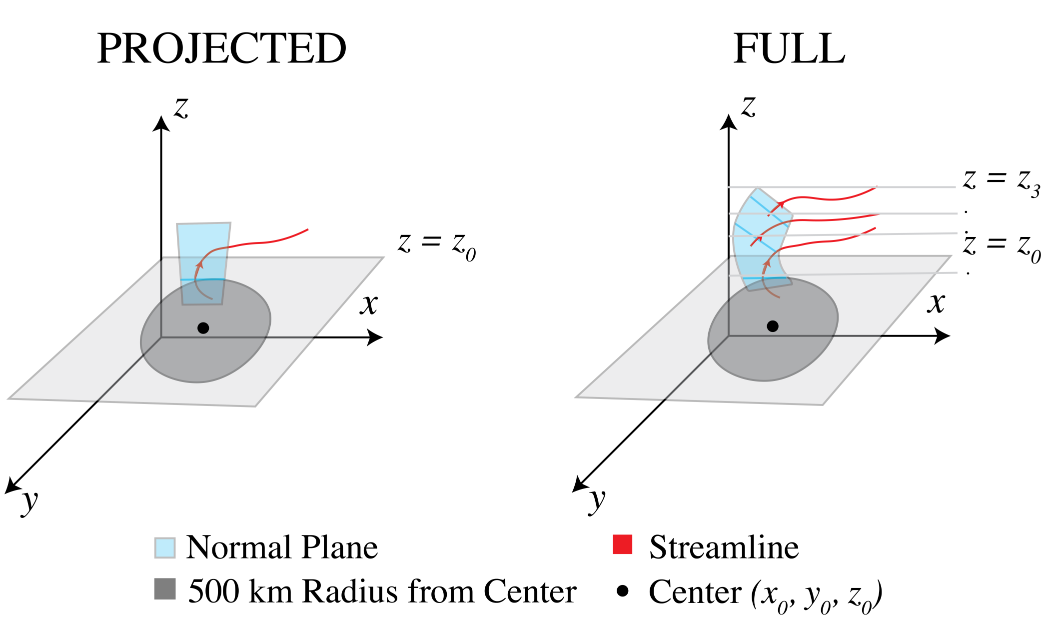

FIG. 7. Schematic diagram of different planes identified for the two versions. Here x is longitude, y is latitude, and z is pressure (hPa, descending). The red streamlines are fixed to the horizontal plane at a particular height z. The PROJECTED version of the algorithm uses only one pressure to identify the jet, z_0, whereas the FULL version uses multiple pressure levels with corresponding mass flux, $(z_0, ..., z_3)$.

In the PROJECTED version, where mass flux is calculated according to the flow vectors associated with the original streamline, the jet identified will be that with maximum mass flux at any level in the direction of that particular streamline (Fig. 7). In contrast, in the FULL version, mass flux is computed with respect to the specific flow vector at each level.

3. *Finding the Rest of the Cross Sections*

The procedure described in the previous section is repeated, looping through the points on the initial streamline(s) in order to re-form the search space for the normal plane, and using the horizontal wind vector at those points to determine which points within the search space are on the normal plane. Then, the mass flux is computed over all points within the normal plane, and the points with mass flux above a certain threshold, but yielding a total mass flux approximately equal to that of the initial cross section, are selected as the jet cross section.

Initially, points that have mass flux at least 80% of the maximum within the search space, the normal plane, and that are close to the initial streamline point, are considered as the next jet cross section. If those points do not represent total mass flux equal to that of the initial cross section, then points that are successively farther away from the initial streamline point, but within the normal plane, and points with successively lower amounts of mass flux (as low as 40% of the maximum) are considered. The documentation describes the precise search procedure, the errors that may arise when the search procedure fails, and what those errors indicate about the existence of the jet.

For most cases, the PROJECTED version is sufficient to identify the jet, as the flow in the relevant layers of outflow does not significantly differ in direction. For instance, during the period in which Hurricane Laura attained maximum intensity, the forecasted dominant flow at and around the level of maximum divergence is initially north-northeast (§3). However, the FULL version of POJ3 is available in cases where a POJ may ascend outside the 500 km radius or appear to split off, i.e. fan in different directions at each level, due to, say, the influence of an upper tropospheric trough (UTT). An example of this is Hurricane Irma on 1800 UTC September 9, 2017 (Fig. 8). Here, the initial streamline at 175 hPa and that at 225 hPa begin in a similar location but diverge in their trajectories, with the lower streamline going northward towards the UTT and the higher streamline becoming drawn into an anticyclone that developed between Hurricanes Irma and Jose. In this case, it is not sufficient to use the flow direction at the level of maximum divergence to approximate that of all relevant pressure levels since the upper level flow is dominated by the influence of an anticyclone to the southeast, while at lower levels in the outflow layer, the flow is dominated by the influence of a UTT. Using the FULL version, each of the streamlines, which eventually diverge, can effectively be traced, forming a jet that can "split off" at different levels. When using the FULL version, it may be preferable to select values over only part of the outflow layer, as the POJs identified in this study have remained concentrated over only a subset of the typical 300 hPa-100 hPa possible extent of the outflow layer.

2) Two Jets

Mature tropical cyclones have been observed to form two POJs rather than one in some cases (Wu and Emanuel 1994). Since not all TCs have two jets, the default version of POJ3 only searches for one jet. The two-jet version essentially repeats the process (either PROJECTED or FULL) described in the previous section twice, with the streamline(s) used to find the first jet disqualified from the set of potential streamlines to choose.

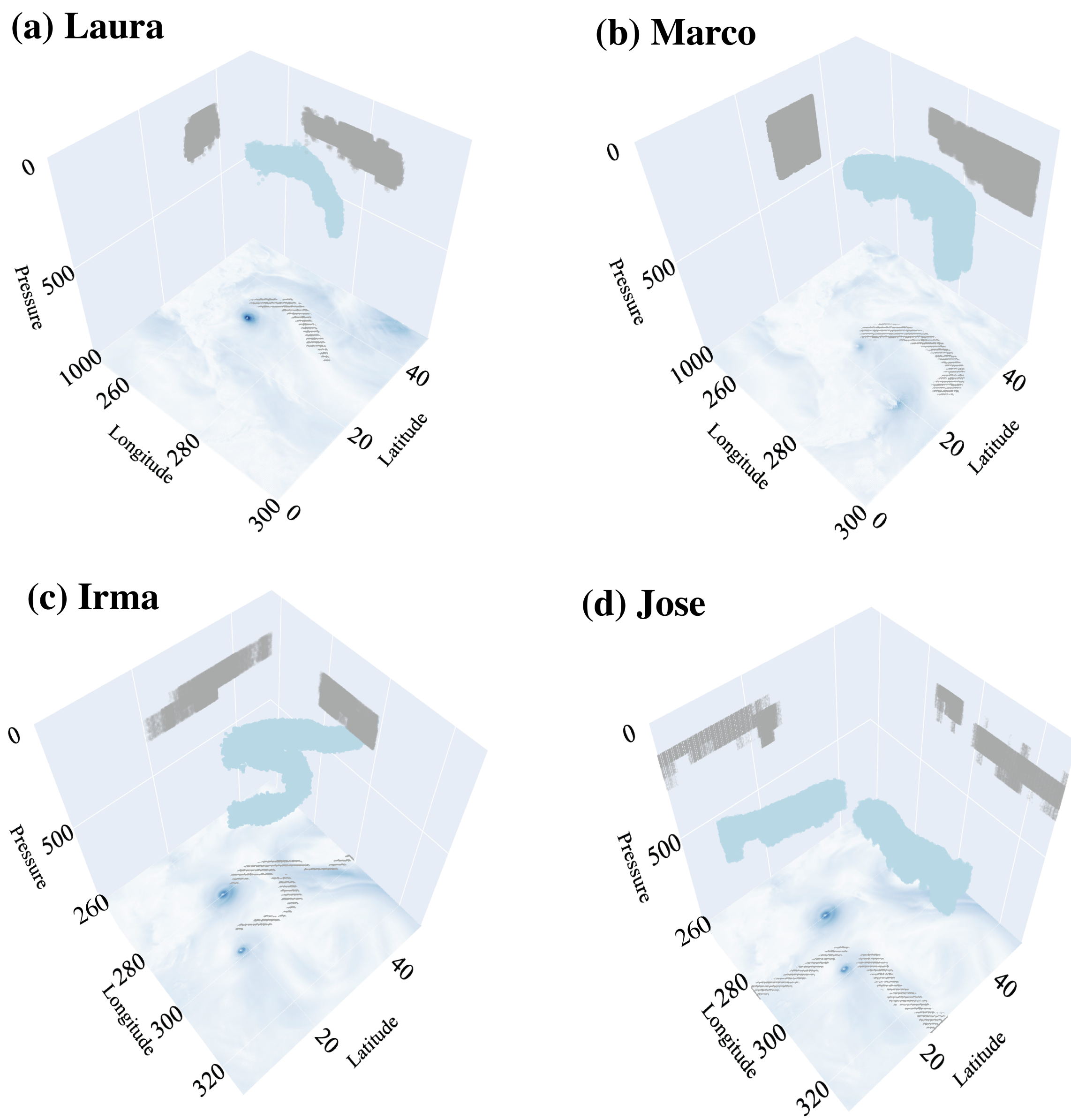

FIG. 8. The jets identified by POJ3, in 3 dimensions – longitude, latitude, and pressure (hPa). Each jet is shown using a point cloud with random jitter added on the pressure axis in order to smooth over the discrete pressure levels available in the data. The gray portions on each coordinate plane are shadows of the 3D jet (light blue). The longitude-latitude plane features the approximate surface wind speed (at 875 hPa, with darker colors meaning higher speed) computed using the same data. **(a)** Laura: HWRF, initialized 0000 UTC August 27, 2020, valid time 0300 UTC, 0.25 degree horizontal grid spacing and 25 hPa vertical spacing. **(b)** Marco: HWRF, initialized 0600 UTC August 23, 2020, valid time 0900, 0.25 degree horizontal grid spacing and 25 hPa vertical spacing. **(c)**, **(d)** Irma and Jose: GFS, initialized 1200 UTC September 9, 2017, valid time 1800, 0.25 degree horizontal spacing and 50 hPa vertical spacing.

3. Case Studies

Two pairs of binary tropical cyclones, Hurricanes Laura and Marco (2020) and Hurricanes Irma and Jose (2017), were used as test data for POJ3 and as case studies on the outflow interactions between TCs. Hurricanes Laura and Marco were initially chosen for this study due to the availability of HMON and HWRF forecast data, which have a finer vertical grid spacing than archived GFS data (25 hPa vs. 50 hPa), and because their proximity allowed for potential outflow interactions (Fig. 9). Hurricanes Irma and Jose were chosen as a second case study because the algorithm showed that during the period of co-existence, only Marco and not Laura had developed a POJ. In contrast, Hurricanes Irma and Jose were more intense during their period of co-existence, such that they developed outflow jets at the same time. The jet locations and strengths, found using POJ3, indicate periods in which outflow interactions could align with anomalous track behavior by Hurricane Jose.

Using forecast data from these TCs also enabled the validation of the results from POJ3 by comparing the location, size, and surrounding environmental fields of the identified POJs to that which would be expected based on prior studies.

a. Hurricanes Laura and Marco

1) Synoptic History

Hurricane Marco and the storm that became Hurricane Laura were both in the Atlantic basin for five days in late August 2020 (Fig. 9). The two TCs originated from tropical waves that formed off the coast of Africa in mid-August. While in the Atlantic basin, Marco led northwest of Laura. As of August 21, Marco had become more organized and had sufficiently fast maximum sustained surface winds to be classified as a tropical depression (Beven and Berg 2021). Around 1300 UTC August 21, Tropical Depression Thirteen was upgraded to Tropical Storm Laura (Brennan 2020). At 0000 UTC on August 22, Tropical Depression Fourteen intensified to Tropical Depression Marco. The following day, Marco intensified further, becoming a category 1 hurricane. Laura also strengthened into a tropical storm during this time, making landfall in the Dominican Republic with an intensity of approximately 45 kt, while Marco was over the southeast Gulf of Mexico (Pasch et al. 2021; Beven and Berg 2021). A low-level ridge northeast of Marco was a major steering influence for both storms (Fig. 10). Around 0000 UTC on August 25, Marco encountered strong vertical wind shear and degenerated into a remnant low and then a trough near the coast of Louisiana (Beven and Berg 2021). Laura made landfall in western Cuba at the same time.

As Laura emerged over the Gulf of Mexico, sea surface temperatures were conducive to intensification. The storm did not follow the same northward track as Marco and avoided the region of high vertical wind shear associated with the jet stream. As a result, Laura reached hurricane strength around 1200 UTC on August 25. Hurricane Laura then underwent rapid intensification until 0000 UTC August 27, reaching a peak intensity of category 4. About six hours later, Laura made landfall in Louisiana. Hurricane Laura caused an estimated \$19 billion of damage in the United States (Pasch et al. 2021). Though the track and genesis of Laura were well-predicted with average forecast errors, the rapid intensification on August 26 was not adequately captured by predictive models (Pasch et al. 2021).

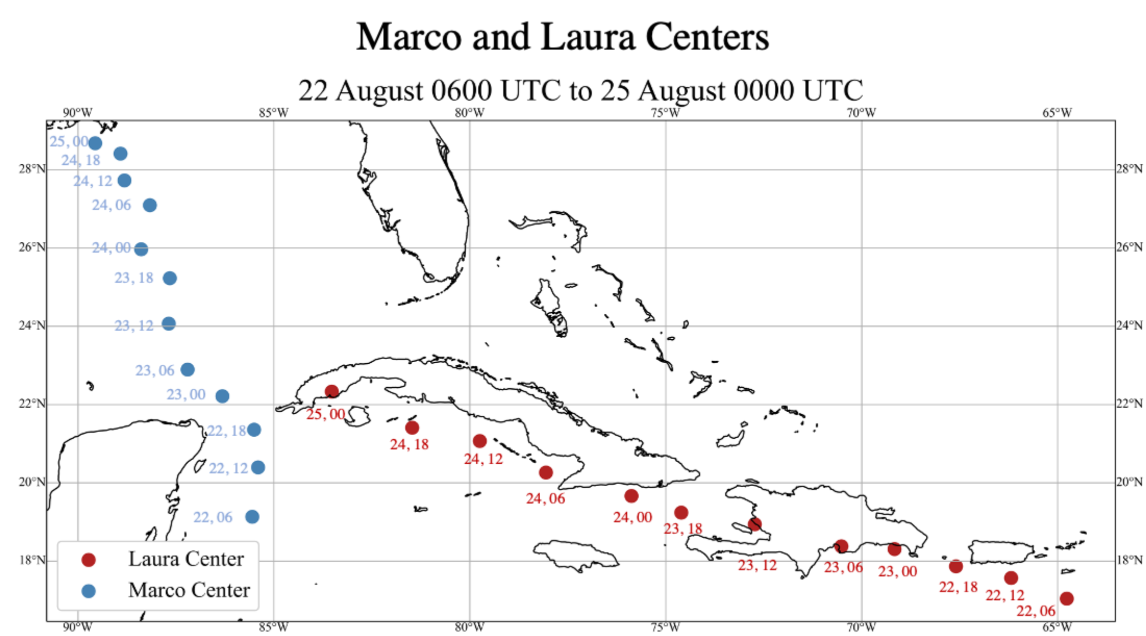

Fig. 9. Tracks for Laura and Marco during the period of coexistence in the Atlantic basin. The points are labelled by the corresponding date, with the convention DD, HH where DD is the day in August 2020 and HH is the valid time of the forecast in UTC. The center locations were found using the geopotential centroid method. The data used were HWRF output, initialization time same as valid time, 0.25 degree horizontal grid spacing (global grid) with 25hPa vertical grid spacing.

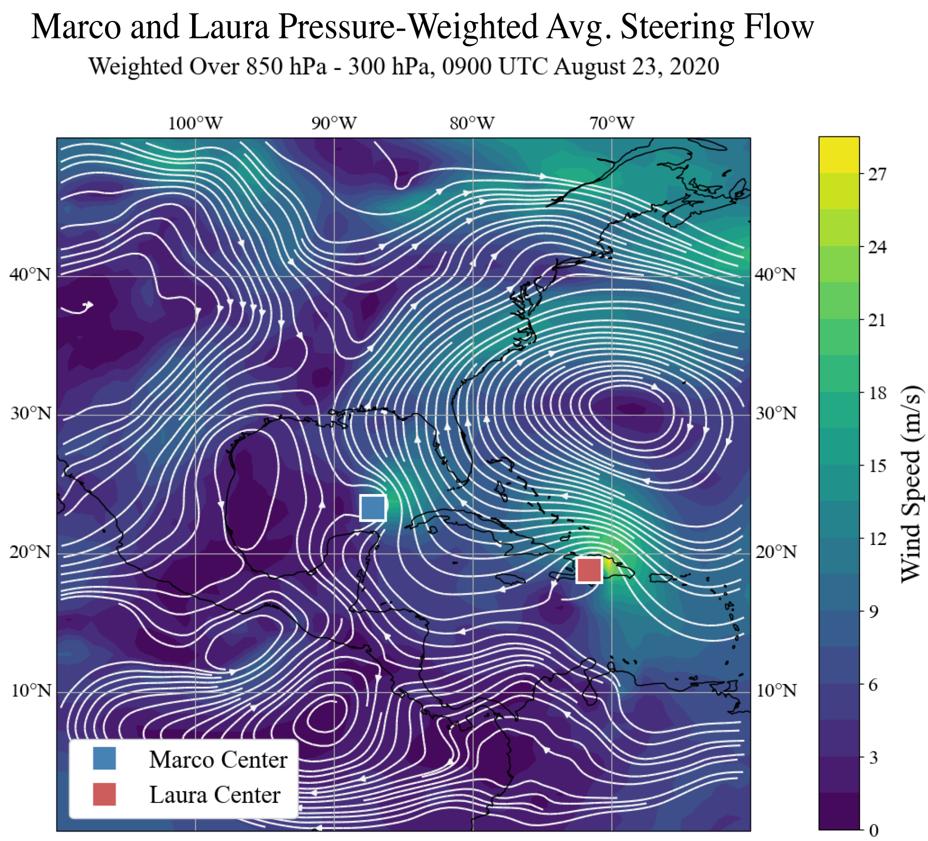

399 FIG. 10. Synoptic environment for Marco and Laura, showing their centers, and 850 hPa-300 hPa layer average steering flow. The data used were HWRF output, initialized 0600 UTC August 23, 2020, valid time 0900 UTC August 23, 2020, with 0.25 degree horizontal grid spacing.

2) DATA

The data used for the analysis of Hurricanes Laura and Marco were primarily produced by the National Center for Environmental Prediction (NCEP) Hurricane Weather Research (HWRF) model. The relevant repository is the NOAA Operational Model Archive and Distribution System (NOMADS) at NCEP. HWRF has had continual upgrades since it first became operational in 2007 (Mehra et al. 2018).

Data from this model were downloaded in near real-time while the storms were active. A 126-hour forecast initialized at 6-hour intervals was provided, with coincident forecasts available for Hurricanes Marco and Laura initialized from 0600 UTC on August 22, 2020 UTC to 0000 UTC on August 25, 2020. For Hurricane Laura, forecasts were available initialized through 0000 UTC

August 27, 2020. For POJ3 and all pre-processing steps, the coarsest grid spacing from the model, which was 0.25 degree horizontal grid spacing, was used, so that both Marco and Laura were within the domain of the model. Forecast hour 0 was preferable for the analysis as it was closest to the initialized time, however, the vertical velocity was identically zero for these time steps, so forecast hour 3 was used.[3] The forecast initialized at 0000 UTC August 27, 2020 was used to identify the POJ when Hurricane Laura was in its later stages and for the analyses done in §3.c.

The only exception was that for the HYSPLIT trajectories in Fig. 14, archival data from GFS were used, due to the unavailability of HWRF data in the HYSPLIT web interface.[4]

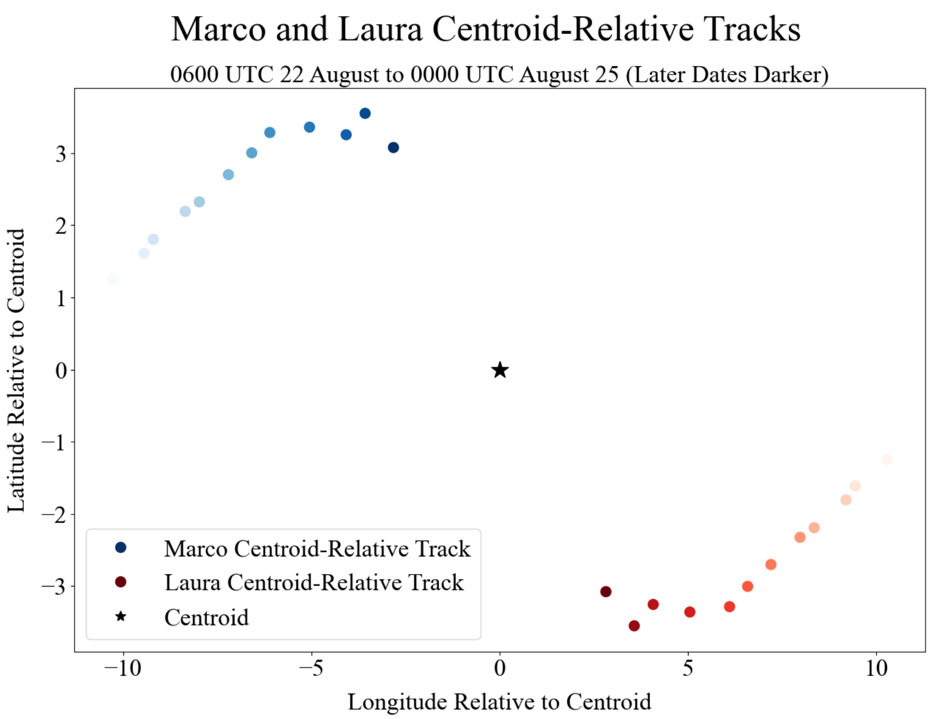

FIG. 11. Tracks for Marco (blue) and Laura (red), with respect to their centroid (black). Centroid-relative tracks were computed using the same centers as in Fig. 10.

[3]Approximately 4% of the horizontal velocity data were missing in the forecast hour 3 data, primarily for the southeast corner of the relevant domain. To run POJ3, it was necessary to fill in the missing data, for which linear interpolation was used. Although a method specifically for extrapolation should be used for any data missing at the corners of the grid, in this case, none of the streamlines involving points at the corner of the grid qualified as the initial streamlines, so this would make no actual difference in the calculation of the POJ.

[4]As this analysis was primarily for heuristic purposes, the available (GFS) data were sufficient.

3) Analysis of Centroid Relative Motion

To eliminate the possibility of direct binary TC interactions as a confounding variable in the analysis of outflow interactions, an analysis of centroid relative motion was performed for Hurricanes Laura and Marco, as in Lander and Holland (1993). There have been instances of Fujiwhara interaction at similar separation distances to those between Marco and Laura (Dong and Neumann 1983). The centroid-relative tracks of TCs undergoing a Fujiwhara interaction would be expected to show first anticyclonic motion about the centroid, followed by cyclonic motion that approaches the centroid (Carr et al. 1997). The cyclonic motion about the centroid has been considered a defining feature of direct binary TC interactions (Carr et al. 1997).

The centroid-relative motion for Marco and Laura is shown in Fig. 11. Although there was some anticyclonic centroid-relative motion, there was no significant cyclonic rotation about the centroid. Thus, we conclude that a mutual, direct interaction, such as a classical Fujiwhara interaction, did not occur between Marco and Laura.

4) Outflow Interactions

As a first step to determine whether there were any significant interactions between the outflows of Laura and Marco, the vertical extents of their outflow layers were determined. During the period of their coexistence in the Atlantic basin, Marco and Laura's outflow layers generally spanned over the same range of vertical levels, indicating the potential for outflow interactions (Fig. 12). Marco underwent a short period of intensification beginning on 0600 UTC August 23, so we ran POJ3 for both Marco and Laura on forecast data initialized at this time[5] to determine whether there were any significant outflow interactions coinciding with the period of intensification. We also tracked the trajectory of Marco's POJ in order to assess whether it could have contributed in any way to Laura's steering flow, since Laura proceeded into the Gulf of Mexico after Marco degenerated. During the period of coexistence, Marco did reach hurricane strength, with maximum sustained surface winds of at least 33 m s^{-1}, which is sufficiently strong to support the formation of an outflow jet. For instance, Shi et al. (1990) found that an outflow jet formed in simulations even for a weak storm, with maximum surface winds of 23.2 m s^{-1}. The PROJECTED single jet version of POJ3 was run for both Marco and Laura at this time step.

[5]Forecast hour 3 was used.

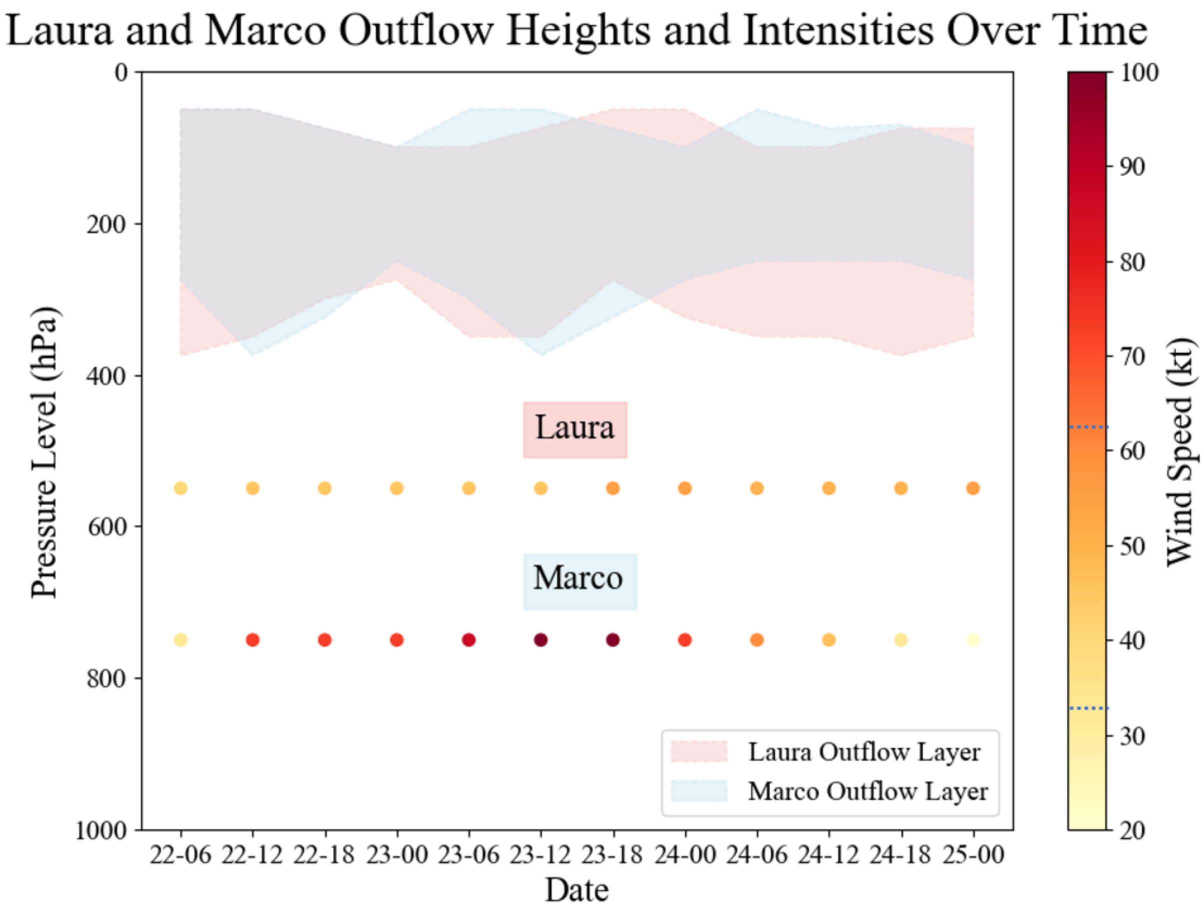

FIG. 12. The outflow layer heights of Marco and Laura during the time-steps in which they coexisted in the Atlantic basin, determined per the (area-weighted) divergence method. HWRF data with 0.25 degree grid spacing were used to compute the corresponding heights. Below, the colored circles show the wind speed in knots at each time step according to the NHC reports for Laura and Marco as a reflection of the intensities of the TCs (Pasch et al. 2021; Beven and Berg 2021). The points are labelled by the corresponding date, with the convention DD, HH where DD is the day in August 2020 and HH is the valid and initialization time of the forecast in UTC. The lower blue dashed line in the colorbar marks the minimum wind speed for the classification as a tropical storm (34 kt) and the higher blue dashed line marks the minimum wind speed for the classification as a hurricane (64 kt) per the NHC.

Marco developed a northern jet going towards the UTT, as one may expect (Komaromi and Doyle 2017) (Fig. 13). The initial cross-section of this jet at a radius of 500 km was a well-defined region of concentrated mass flux (Fig. 6), whereas no such region could be identified for Laura.

This combined with the fact that there were insufficient points that met the search criteria and that conserved the initial mass flux amount suggests that Laura did not have a well-developed outflow jet at this time, which may be expected since Laura was not particularly well-organized or intense.

The northward trajectory of Marco's jet meant it did not intersect with Laura's outflow layer. The trajectory of Marco's jet and the lack of a well-developed jet for Laura suggest that Marco and Laura did not have any direct outflow interactions at the 0900 UTC August 23 time step, and subsequent time steps gave similar results.

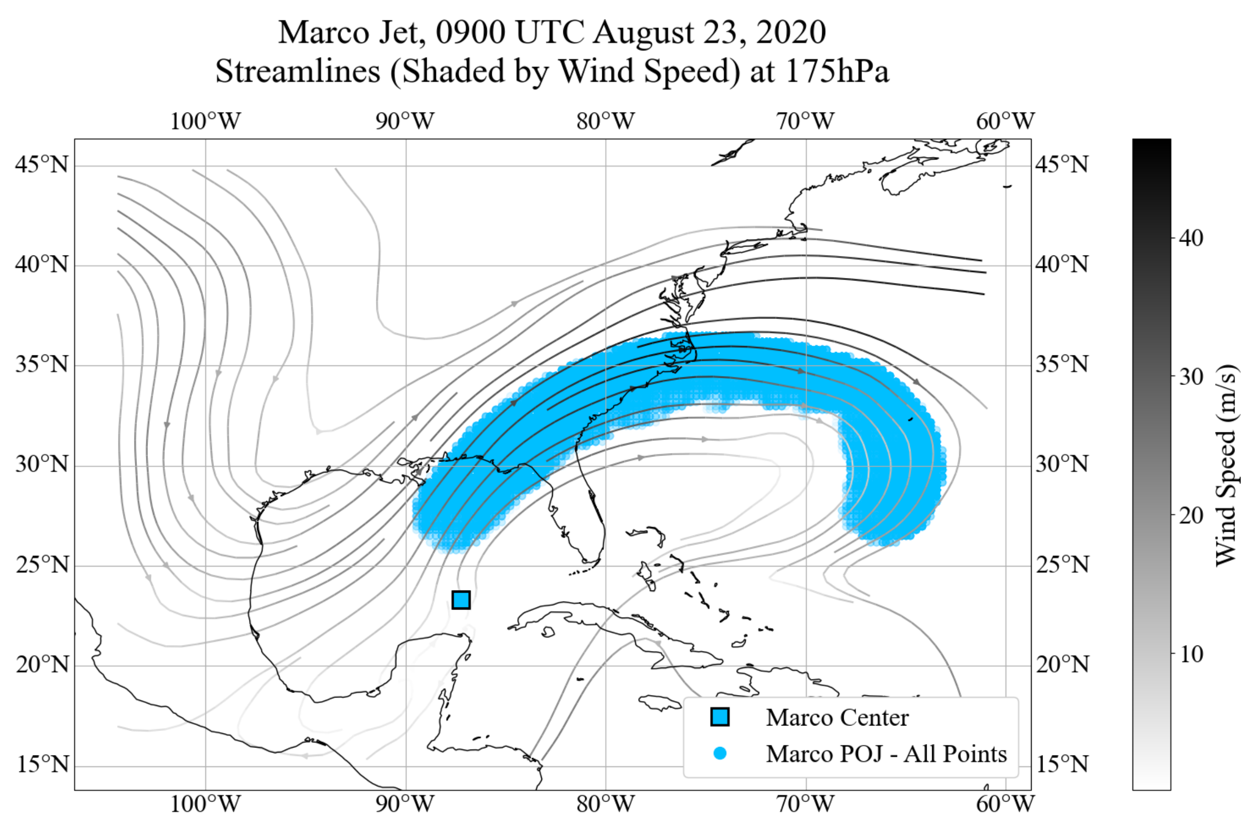

FIG. 13. A bird's eye view of the points associated with the outflow jet for Marco (shaded in blue), at 0900 UTC August 23, 2020, produced by the single-jet POJ3 PROJECTED version initialized at the level of maximum divergence of 175 hPa and ran to 3000 km in length (HWRF, initialized 0600 UTC August 23, 2020, valid time 0900 UTC August 23, 2020, 0.25 degree horizontal grid spacing).

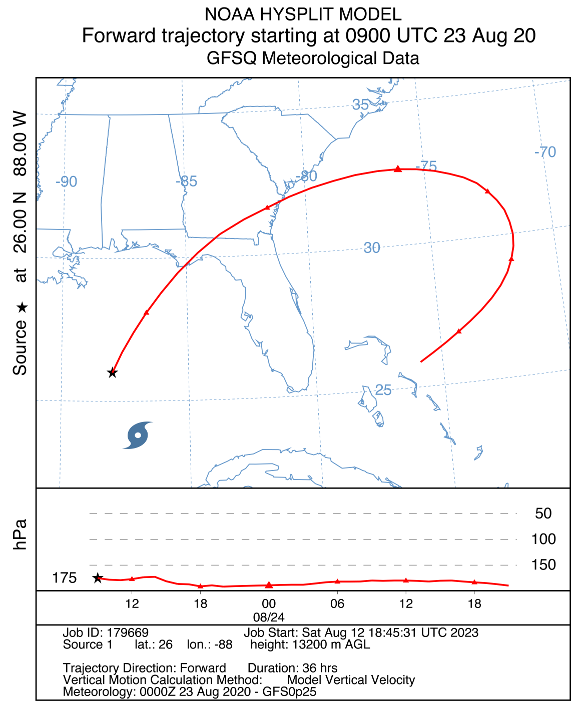

FIG. 14. Output from HYSPLIT near Hurricane Marco beginning at (valid time) 0900 UTC August 23, 2020. TC center at this time marked in blue. GFS data, initialized 0000 UTC August 23, 2020, 0.25 degree horizontal grid spacing. Produced using the web interface version of HYSPLIT (Stein et al. 2015; Rolph et al. 2017).

However, an examination of the steering flow (Fig. 10) shows there was a significant anti-cyclone between the two storms. This ridge was in this region even before the storms entered it, and was identified as a significant steering influence for both storms (Beven and Berg 2021; Pasch et al. 2021). Additionally, the trajectory of Marco's POJ is such that some of the outflow could potentially propagate around the ridge, possibly strengthening it and indirectly steering Laura. To test this hypothesis, it was necessary to trace specific outflow air parcels further in time. The NOAA Hybrid Single-Particle Lagrangian Integrated Trajectory (HYSPLIT) model, which can compute the trajectory of air parcels for archival data, was used (Stein et al. 2015; Rolph et al. 2017). The parcels were initialized (approximately) in Marco's POJ, and indeed, as shown in Fig. 14, some parcel trajectories traverse the ridge and exit directly where Laura's center was located. Thus, while this pair of binary TCs featured no discernible direct outflow interactions, the results suggest that an indirect outflow - TC interaction, in the vein of the indirect interactions described in Carr et al. (1997), may have occurred.

b. Hurricanes Irma and Jose

1) Synoptic History

Irma and Jose both formed from tropical waves off the west coast of Africa, on August 27, 2017 and August 31, 2017, respectively. The best track data for Irma and Jose during their period of coexistence in the Atlantic basin are shown in Fig. 15. Irma became a tropical depression around 0000 UTC on August 30 while near the Cabo Verde Islands. Only two days after cyclogenesis, Irma underwent rapid intensification and became a major hurricane by 0000 UTC September 1. Over the next three days, Irma fluctuated between category 2 and 3. In the early hours of September 5, Jose also became a tropical depression near the Cabo Verde Islands after following a similar path. As Jose crossed the Atlantic, it was steered northward by a mid-tropospheric ridge, arriving near the Leeward Islands where there were warm sea surface temperatures and mild vertical wind shear. At this point, Irma was near Barbuda and approaching its peak intensity of 155 kt. By 1800 UTC on September 6, Jose had become a hurricane, and Irma was making landfall as a category 5 hurricane in Barbuda. Irma's landfall on Barbuda caused three direct deaths and an estimated $150-300 million (USD) in property damage, and destroyed 95% of Barbuda's infrastructure (Cangialosi et al. 2021; Berg 2018). In anticipation of a second landfall by Hurricane Jose, most residents of Barbuda were forced to evacuate, eventually causing the island to become uninhabited. The intensity of Jose subsequently increased from 50 kt to 135 kt, as it headed towards Barbuda. As of 1800 UTC on September 9th, 2017, a tropical storm warning for Barbuda was in effect (Ballard and Brown 2017b). However, on late September 9, Jose turned northwestward, narrowly missing Barbuda. By 2100 UTC on September 9th, 2017, the tropical storm warning had been discontinued (Ballard and Brown 2017a). This was attributed to a weakness in the subtropical ridge partially due to Hurricane Irma, which was over Florida at this time, in the NHC Hurricane Jose report (Berg 2018).

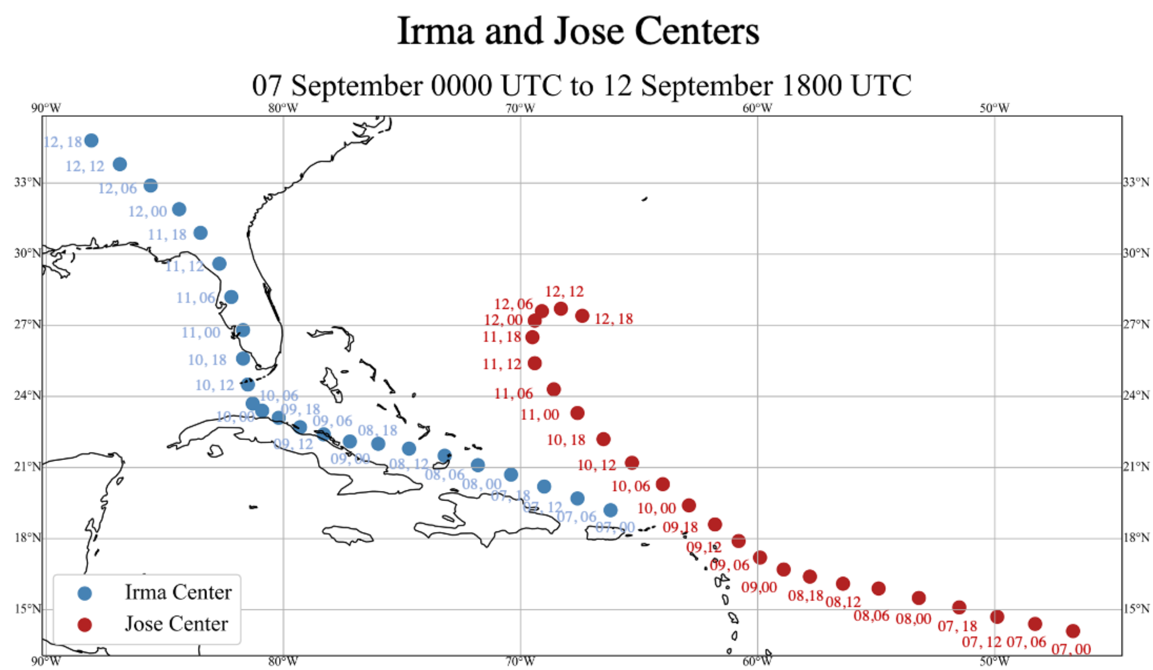

FIG. 15. Tracks for Irma (blue) and Jose (red) during period of coexistence in the Atlantic basin. Centers are from best track data from the National Hurricane Center reports for Irma and Jose, respectively (Cangialosi et al. 2021; Berg 2018). The points are labelled by the corresponding date for each center location, with the convention DD, HH where DD is the day in September 2017 and HH is the time in UTC.

Early on September 9, Irma made its fifth landfall, near Cuba, causing it to eventually weaken to a category 2 hurricane. Upon entering the Florida Straights, Irma strengthened to a category 4 hurricane, later making landfall in the Florida Keys. As Jose moved northwestward, it entered a region of greater northeasterly shear, which together with a partial eyewall replacement cycle caused its inner core to collapse and its intensity to weaken below that of a major hurricane. As of late September 11th and early September 12th, Irma was a tropical storm over Florida, and Jose was trapped between the large cyclonic circulation associated with Irma and a mid-latitude closed low off the coast of Canada. As a result, Jose followed an unusual, clockwise loop while in the Atlantic. At this point, Irma degenerated into a remnant low. After the loop, Jose re-intensified, but was met with high vertical wind shear and cold waters north of the Gulf Stream, which made it weaken and eventually dissipate (Berg 2018).

2) Data

Archival data from the Global Forecast System (GFS) run by the U.S. National Weather Service were primarily used for the analysis of outflow interactions between Hurricanes Irma and Jose. The GFS is re-initialized four times each day, producing hourly forecasts for the following 120 hours. For the purposes of this study, we wanted to analyze data valid at 1800 UTC on September 9th, 2017, as this directly preceded the time of interest. It was desirable to have data initialized as close to this time as possible, and the best available data were initialized at 1200 UTC on September 9th, 2017. The current version of GFS uses the Finite-Volume Cubed-Sphere Dynamical Core (FV3), making it a nonhydrostatic model as of 2019, but the data for Irma and Jose were generated while the GFS was still hydrostatic (2017). Although the data were generated using the spectral method in the dynamical core, they were generated just after the preceding major upgrade (July 2017) of the GFS. The horizontal grid spacing is 0.25 degrees and the vertical grid spacing is 50 hPa. The only exception was that for the HYSPLIT trajectories in Figure 17, archival data from the Global Data Assimilation System (GDAS) with 0.5 degree grid spacing were used, as these were the best available in the HYSPLIT web interface. Additionally, center locations for the storms were taken from the best track data in the National Hurricane Center reports for Irma and Jose, respectively (Cangialosi et al. 2021; Berg 2018).

3) Analysis of Centroid Relative Motion

As for Laura and Marco, the centroid-relative tracks for Irma and Jose were plotted per the method described in Lander and Holland (1993) (Fig. 16). The centroid-relative tracks do not show the cyclonic rotation about the centroid that is characteristic of direct binary interactions between TCs (Carr et al. 1997). No such binary interactions were recorded in the NHC meteorological history reports either (Cangialosi et al. 2021; Berg 2018). Thus, as in the case of Laura and Marco, we conclude that a Fujiwhara interaction did not occur between Irma and Jose.

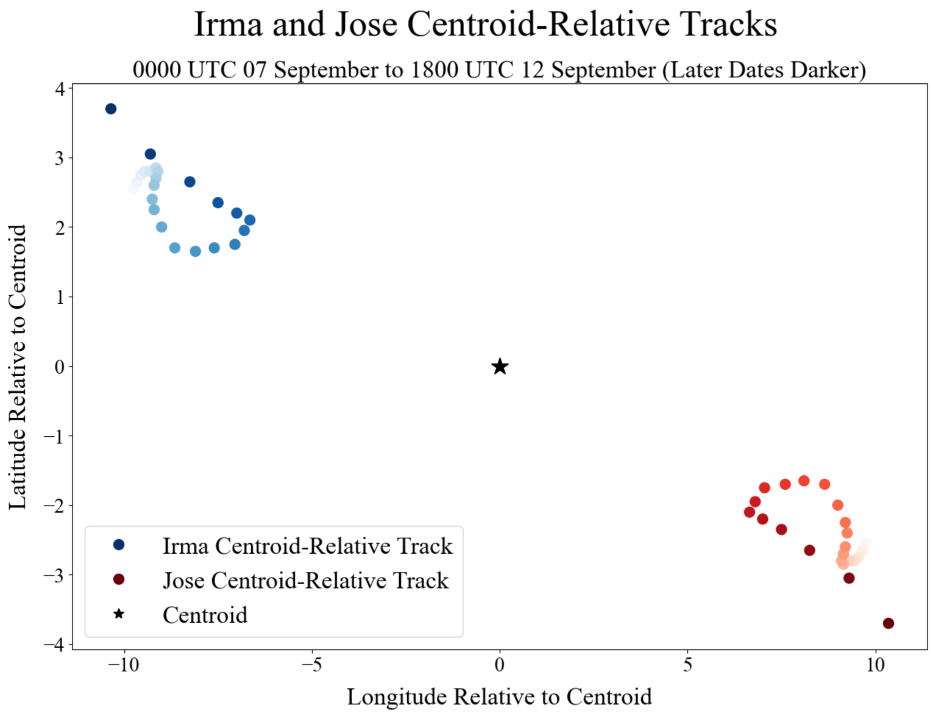

FIG. 16. Tracks for Irma (blue) and Jose (red), with respect to their centroid (black). Centroid-relative tracks were computed using the same centers as in Fig.15.

4) Outflow Interactions

Irma and Jose were selected for their potential for direct outflow interactions, which was supported by a preliminary run of the NOAA HYSPLIT model for parcels initialized in potential locations of Irma's POJ, based on wind speed maxima at 500 km radius from the center. The model output re-initialized at the points that were found to be Irma's POJ as identified by POJ3 is shown in Fig. 17. The pressure-weighted average steering flow in the synoptic environment of Irma and Jose (Fig. 18) suggests a predominantly westward trajectory for Jose that makes landfall over Barbuda, contrary to its actual trajectory, which is more northward (Fig. 15). It is possible that the trajectory of the outflow from Irma arrived west of Jose's center, blocking Jose from heading westward and making landfall on Barbuda, contrary to what was initially anticipated. We investigated this possibility using the POJ3 algorithm.

We found that Irma's POJ and one of Jose's two POJs – all initialized at 175 hPa, the level of maximum divergence for Jose[6] – intersect (Fig. 19). The collision of the POJs is a direct

[6]Although the level of maximum divergence for Hurricane Irma was at 225 hPa, the wind speed maximum at this level that also appeared at neighboring pressure levels could be best traced by initializing at 175 hPa: see documentation.

interaction between the outflows of Irma and Jose. This interaction suggests that the northward turn that Jose took late on September 9th – which was attributed in the NHC report to a weakness in the subtropical ridge caused by Hurricane Irma — may be better described as a turn due to the presence of a high pressure system created by the intersection of the POJs. This is similar to the ”blocking effect” described in Ryglicki et al. (2019), created by the collision of the outflow and environmental winds, and can likewise be viewed in terms of the diversion of Bernoulli flow about an obstacle. This diversion away from Barbuda was not predicted, and the residents of Barbuda had evacuated as a result. Had there been the capacity to identify these POJs at the time, it is possible that Jose's turn away from Barbuda could have been predicted.

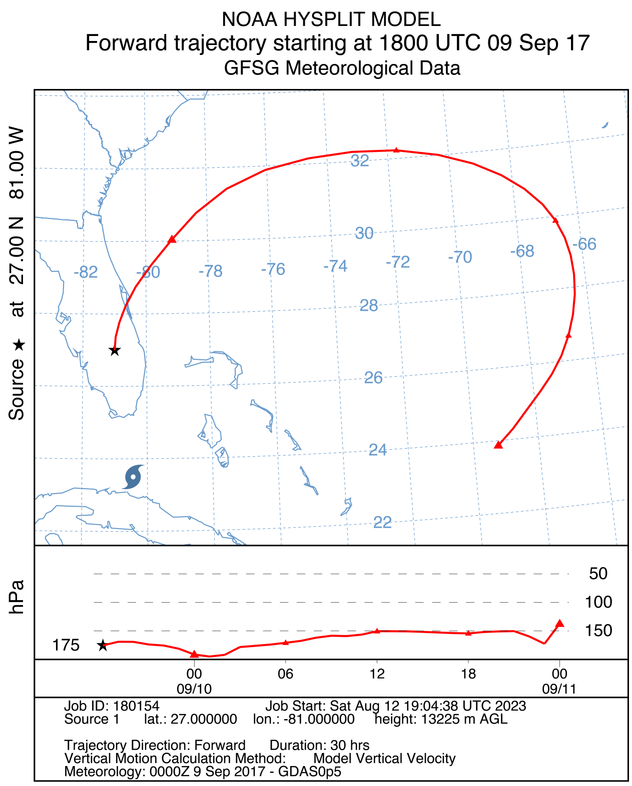

FIG. 17. HYSPLIT trajectories for points initialized approximately in Irma's outflow jet, beginning at (valid time) 0600 UTC 9 September 2017. TC center at this time marked in blue. GDAS data with 0.5 degree horizontal grid spacing, initialized 0000 UTC September 9, 2017. Produced using the web interface version of HYSPLIT (Stein et al. 2015; Rolph et al. 2017).

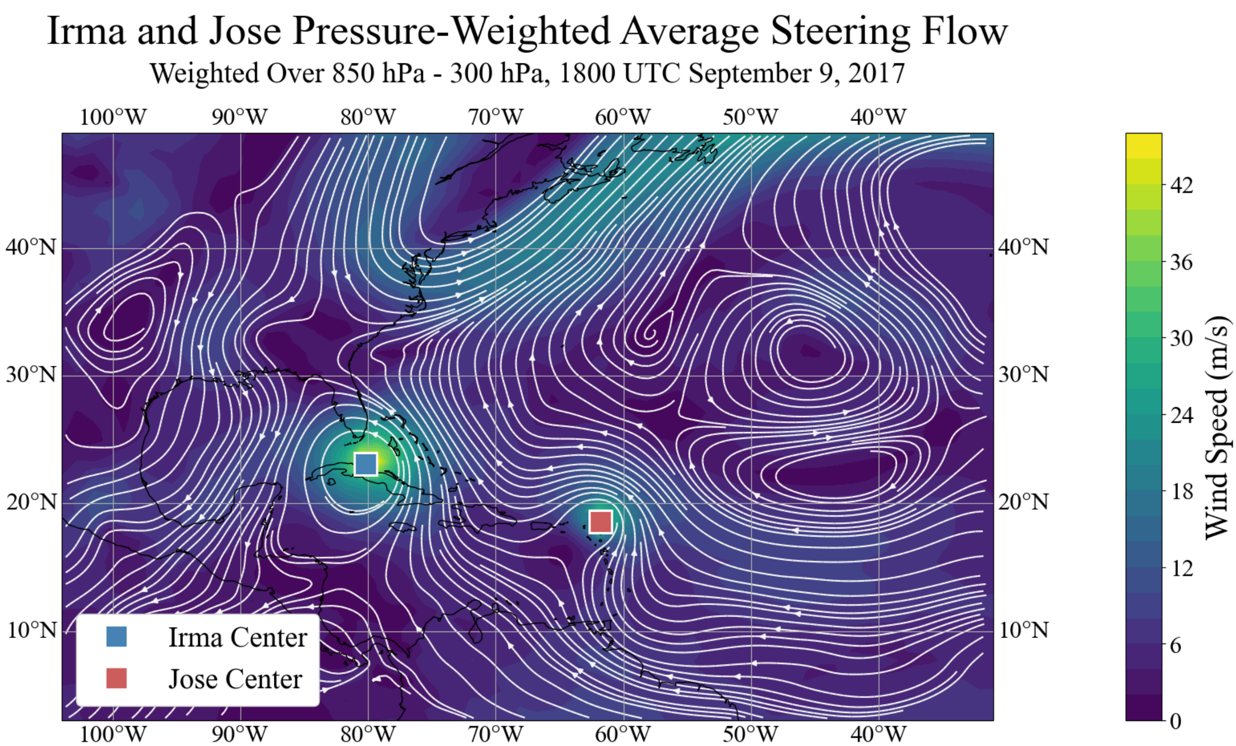

FIG. 18. Synoptic environment for Irma and Jose, showing their centers, and 850 hPa–300 hPa layer average wind (steering flow). GFS data, initialized 1200 UTC, September 9th 2017, valid time 1800 UTC September 9, 2017, 0.25 degree horizontal grid spacing.

We note that when running POJ3 for Irma, the initial streamline computed at the level of maximum divergence for Irma (225 hPa) was inconsistent with the initial streamline at the level above (175 hPa) which was also the level of maximum divergence for Jose. While the streamlines originated in similar locations, the lower streamline went towards the UTT north-northeast of Irma, whereas the upper streamline eventually headed west and southwest towards Barbuda. This suggests that Irma may have had a split jet scenario, due to the competing influence of the UTT to its north, and a strong anticyclone that had formed to its east, between the two storms. Accordingly, the FULL version of POJ3 was run for Irma, tracing the flow individually at the different levels. Additionally, Jose had two strong wind speed maxima at 500 km – one to the North and one to the West. On the other hand, while Irma did have two wind speed maxima at 225 hPa, only one was observed at multiple pressure levels. Consequently, the two-jet version of POJ3 was run only for Hurricane

Jose. The three-dimensional representations of the jets identified for Irma and Jose are shown in Fig. 8 (c-d).

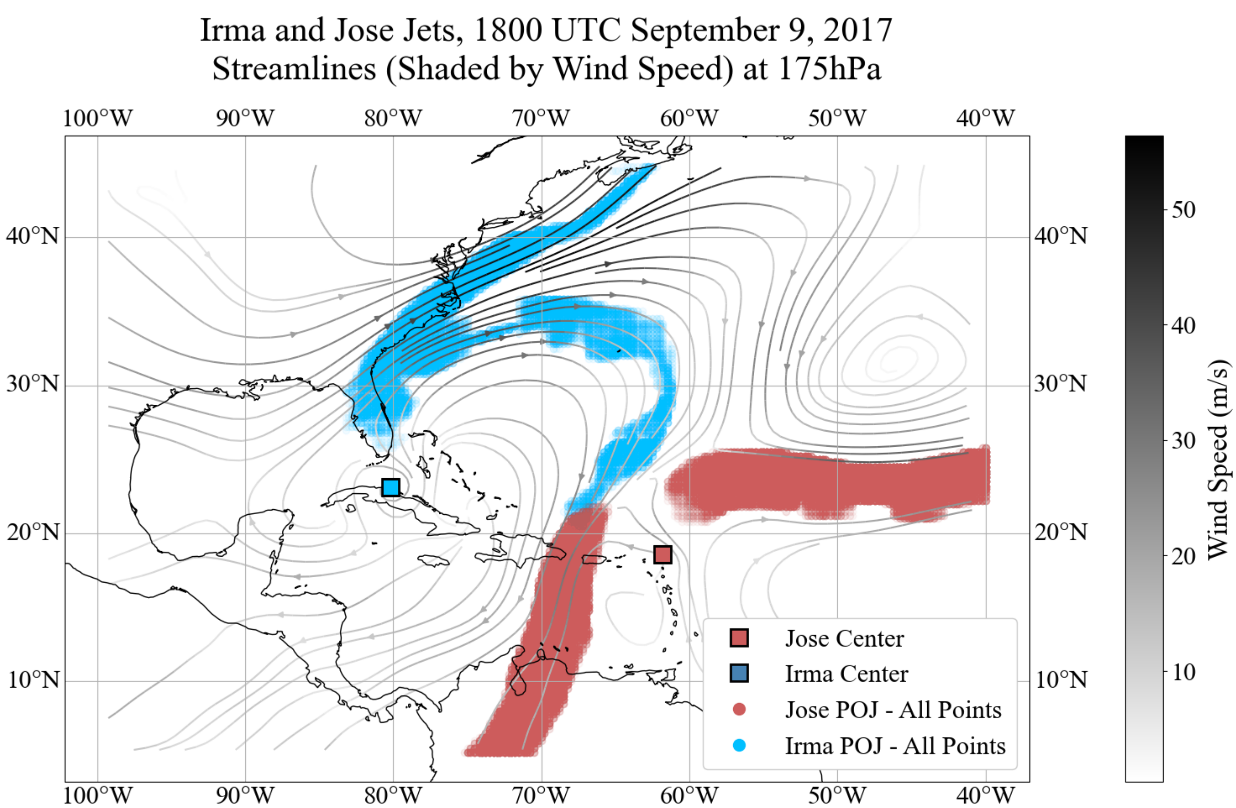

FIG. 19. Jose's POJs, initialized at the level of maximum divergence for Jose, 175 hPa, and Irma's POJ initialized at 175 hPa, on 1800 UTC September 9, 2017. Irma's POJ was used producing the FULL version of POJ3, and Jose's POJs were produced using the two-jet PROJECTED option. Both jets were produced using GFS data, initialized 1200 UTC, September 9th 2017, 0.25 degree horizontal grid spacing. Both jets were run to 3500 km in length (points outside domain boundary not shown).

The case of Hurricanes Irma and Jose illustrates the alignment between outflow interactions and anomalous alterations in TC track, which in turn may affect intensity. For instance, because Jose continued on a northwestward track, not only was a previously-expected landfall avoided, but Jose entered a region of high vertical wind shear which caused its intensity to diminish (Berg 2018). With a better understanding of outflow-outflow interactions, we may be able to predict such previously-unforeseen track changes, and consequently intensity changes, in the future.

c. Alignment of Detected POJs with Prior Results

POJ3 successfully produced POJs that were narrow, long, concentrated regions of flow, which roughly conserved mass flux throughout. Additionally, both the POJ for Marco and the POJ for Irma reflected that the trajectories of outflow jets often form preferentially towards nearby troughs, as tested in simulations by Rappin et al. (2011) and Komaromi and Doyle (2017). It is of interest to see whether signatures in the PV and relative humidity fields also coincide with those found by Shi et al. (1990) and Rappin et al. (2011).

As a test case for POJ3, the data for Laura valid at 0300 UTC August 27, 2020 were used, as at this time step Laura was a category 4 hurricane and high resolution data were available. High resolution forecast output from HWRF was only available for Marco and Laura, and Marco did not attain this intensity. The POJ for Laura at this time step produced by the POJ3 PROJECTED version, computed at the level of maximum divergence of 175 hPa, is shown in Fig. 20. Unlike for Hurricane Irma, which required the FULL version, initializing the POJ3 for Laura at the 200 hPa level produced nearly identical results.

Potential vorticity was computed from the same data that were used in POJ3. Baroclinic potential vorticity was calculated using the MetPy package which implements potential vorticity according to Bluestein (1993):

$$PV = -g\left(\frac{\partial u}{\partial p}\frac{\partial \theta}{\partial y} - \frac{\partial v}{\partial p}\frac{\partial \theta}{\partial x} + \frac{\partial \theta}{\partial p}(\zeta + f)\right)$$

where θ is potential temperature, ζ is the vertical component of relative vorticity, and f is the Coriolis parameter (May et al. 2022). As shown in Fig. 21, the jet was in a region of relatively low PV (<0.5 PVU) in general, and there were negative PV streamers within most regions where the outflow jet was located, at each of the relevant levels. The correspondence with low or negative

PV is especially obvious in the plot at 150 hPa, where a region of higher PV marks the northern boundary of the POJ.

We also compare the POJ location with the relative humidity field at the same levels (Fig. 21). Shi et al. (1990) found that due to the secondary circulation at the jet entrance region, there is high relative humidity (80%) on the anticyclonic shear side of the jet, and low relative humidity ($< 40\%$) on the cyclonic shear side of the jet. At each of the pressure levels, at the entrance region of the POJ for that pressure level, there is high relative humidity on the anticyclonic shear side of the jet and low relative humidity on the cyclonic shear side.

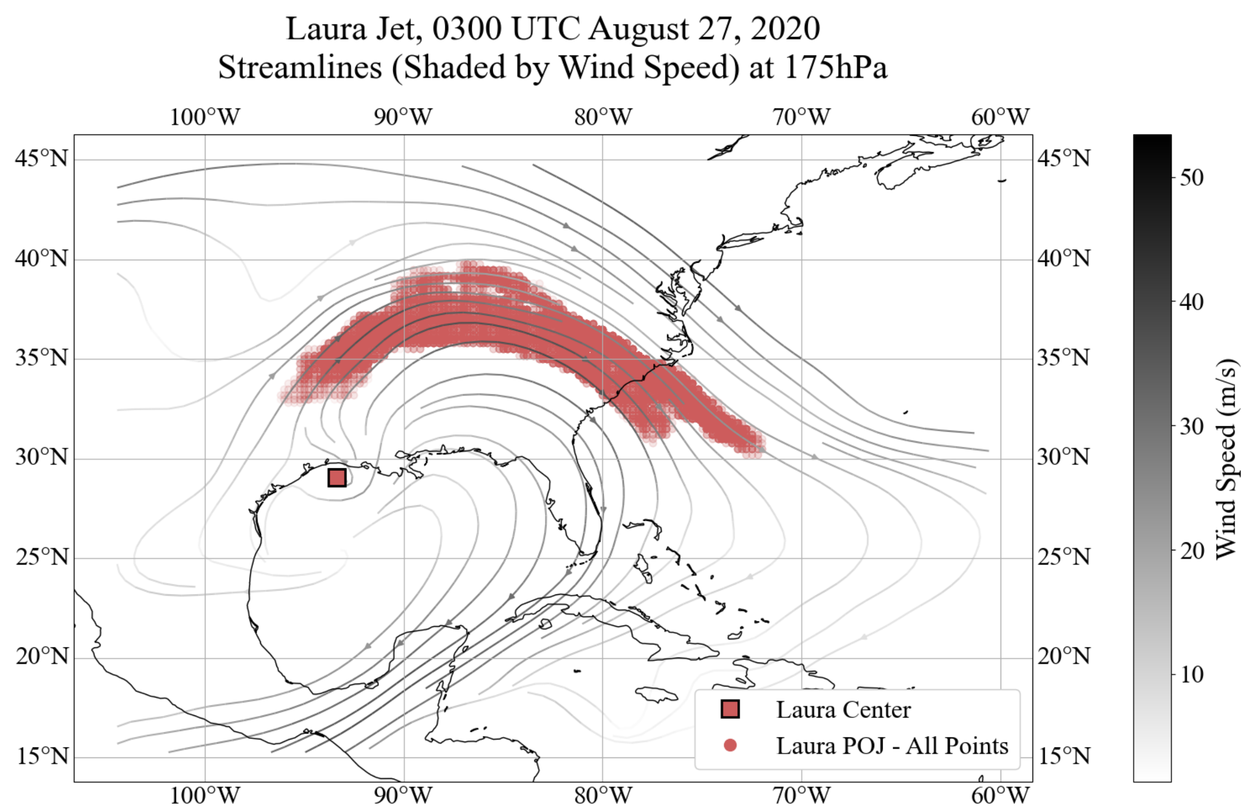

FIG. 20. A bird's eye view of the POJ identified for Laura at peak intensity, initialized at 175 hPa and run to a length of 2500 km. The streamlines and wind speed are also at 175 hPa. The jet was produced using the single-jet PROJECTED version of POJ3, with HWRF data, initialized 0000 UTC August 27, 2020, valid time 0300 UTC August 27, 2020 (forecast hour 3), with 0.25 degree horizontal grid spacing.

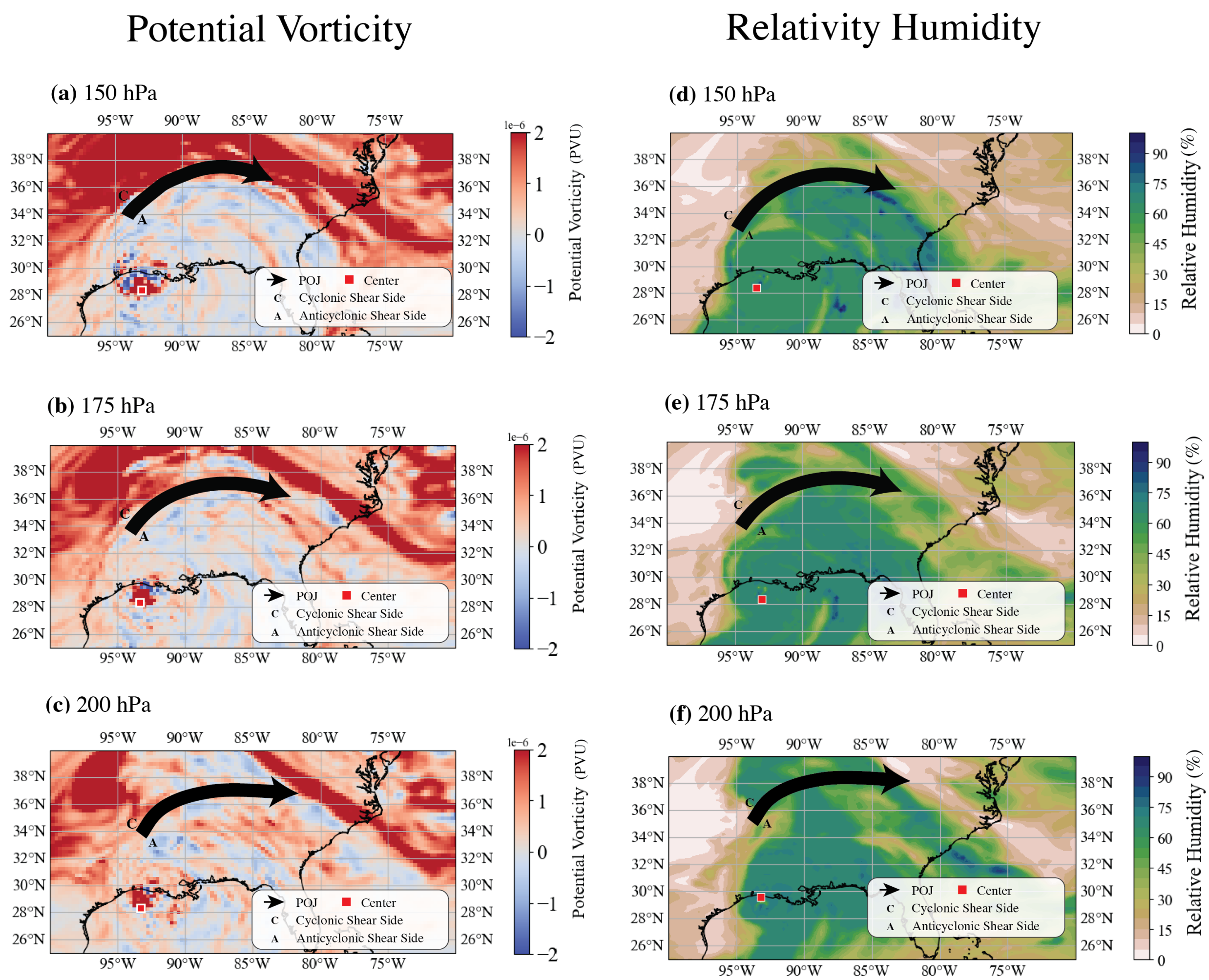

FIG. 21. Left column: potential vorticity in the region surrounding Hurricane Laura near the level of maximum divergence for pressures of **(a)** 150 hPa, **(b)** 175 hPa, and **(c)** 200 hPa. Right column: relative humidity (%) in the region surrounding Hurricane Laura near the level of maximum divergence at pressure levels of **(d)** 150 hPa, **(e)** 175 hPa, and **(f)** 200 hPa. POJ3-identified jet shown as a black arrow, cylconic and anticyclonic sides labeled. HWRF data, initialized 0000 UTC August 27, 2020, valid time 0300 UTC August 27, 2020, with 0.25 degree horizontal grid spacing.

4. Discussion and conclusions

In this study, POJ3, a novel algorithm for identifying the principal outflow jet of a tropical cyclone, has been developed. The locations of the POJs identified by this algorithm, which traces a contour of high mass flux through the outflow layer of a TC, align with prior results concerning the general characteristics of POJs, including the signatures that POJs leave in relative humidity and potential vorticity fields, and how the trajectories of POJs often go towards nearby upper tropospheric troughs. However, despite this alignment, these signatures alone are not distinctive enough to identify the location of POJs with the precision provided by POJ3, highlighting its necessity. POJ3 was applied to analyze outflow interactions between binary TCs for two test cases: Hurricanes Marco and Laura and Hurricanes Irma and Jose. While the location of the identified POJ for Marco and the lack of a POJ for Laura at that time suggests only an indirect outflow - TC interaction occurred for this pair of TCs, the POJs identified for Irma and Jose intersected, suggesting a direct interaction between outflows. The time step associated with the direct outflow interaction was also immediately before an unexpected track change for Hurricane Jose, indicating that this interaction may have played a part in this unpredicted turn. Accordingly, POJ3 can successfully identify POJs and can be useful in analyzing outflow interactions between binary TCs.

However, additional case studies of sets of binary TCs are required to characterize the full range of possible outflow interactions between binary TCs. POJ3 can be used to analyze archived data of binary TCs, or to analyze forecast data from binary TCs that occur in the future. Once a comprehensive classification scheme of different types of outflow interactions has been developed, a theoretical understanding of the dynamics behind them may be more readily pursued.

Of course, the specifics of the POJ3 algorithm may be improved upon in the future. In particular, given access to high quality data for many sets of TCs, the parameters that are left adjustable to the user may be tuned to optimal values. Moreover, if there were high-resolution observational data available that captured an outflow jet, the narrowness and length parameters in POJ3 could be tuned so that the exact shape of the output POJ coincided with that which was observed.

This study has shown that there can be potentially impactful interactions between the outflows of binary TCs, but also demonstrates that this does not happen every time two TCs are sufficiently proximate. What factors are present when TC outflows do interact and the nature of different interactions should be studied further. This POJ-identification methodology holds promise not only for its applicability to further understanding the interactions between binary TCs, but also because its ability to identify a three-dimensional POJ could significantly enhance the understanding of the structure and behavior of TC outflow in general. POJ3 may also be used to make apparent the ways in which TC outflow can interact with other atmospheric systems besides the outflow of another TC.

Acknowledgments. The authors gratefully acknowledge the NOAA Air Resources Laboratory (ARL) for the provision of the HYSPLIT transport and dispersion model and/or READY website (`https://www.ready.noaa.gov`) used in this publication. The authors also wish to thank the Stanford University Sustainability and Earth Summer Undergraduate Research Program (SESUR) for their support of this work. Lastly, the authors deeply appreciate the Sherlock support staff at Stanford University for their assistance with the cluster's computing resources during this research.

Data availability statement. Forecast data for Marco and Laura is available from the last author upon request. The NOMADS data at NCEP may be found at `https://nomads.ncep.noaa.gov/`, and the HWRF data specifically at `https://nomads.ncep.noaa.gov/pub/data/nccf/com/hwrf/prod/`. The GFS data were downloaded from the Research Data Archive managed by the Computational and Information Systems Laboratory at the National Center for Atmospheric Research, and may be obtained from this source upon request. The associated code for POJ3 and its accompanying documentation are available in the Supplementary Materials section.

References

Ballard, R., and Brown, 2017a: Hurricane Jose advisory number 18. NWS Weather Prediction Center College Park MD, URL https://www.nhc.noaa.gov/archive/2017/al12/al122017.public_a.017.shtml.

Ballard, R., and Brown, 2017b: Hurricane Jose intermediate advisory number 17a. NWS Weather Prediction Center College Park MD, URL https://www.nhc.noaa.gov/archive/2017/al12/al122017.public_a.017.shtml.

Berg, R., 2018: National Hurricane Center tropical cyclone report: Hurricane Jose. National Hurricane Center, URL https://www.nhc.noaa.gov/data/tcr/AL122017_Jose.pdf.

Beven, J. L., and R. Berg, 2021: National Hurricane Center tropical cyclone report: Hurricane Marco. National Hurricane Center, URL https://www.nhc.noaa.gov/data/tcr/AL142020_Marco.pdf.

Bluestein, H. B., 1993: *Synoptic-dynamic Meteorology in Midlatitudes: Observations and theory of weather systems*, Vol. 2. Taylor & Francis.

Brand, S., 1970: Interaction of binary tropical cyclones of the western north Pacific ocean. *Journal of Applied Meteorology and Climatology*, **9 (3)**, 433 – 441, https://doi.org/10.1175/1520-0450(1970)009⟨0433:IOBTCO⟩2.0.CO;2.

Brennan, P., 2020: Tropical storm Laura tropical cyclone update. URL https://www.nhc.noaa.gov/archive/2020/al13/al132020.update.08211304.shtml, accessed: 2023-06-02.

Cangialosi, J. P., A. S. Latto, and R. Berg, 2021: National Hurricane Center tropical cyclone report: Hurricane Irma. National Hurricane Center, URL https://www.nhc.noaa.gov/data/tcr/AL112017_Irma.pdf.

Carr, L. E., M. A. Boothe, and R. L. Elsberry, 1997: Observational evidence for alternate modes of track-altering binary tropical cyclone scenarios. *Monthly Weather Review*, **125 (9)**, 2094 – 2111, https://doi.org/10.1175/1520-0493(1997)125⟨2094:OEFAMO⟩2.0.CO;2.

Chavas, D. R., N. Lin, and K. Emanuel, 2015: A model for the complete radial structure of the tropical cyclone wind field. Part I: Comparison with observed structure. *Journal of the Atmospheric Sciences*, **72 (9)**, 3647–3662.

De, S., S. Gupta, V. R. Unni, R. Ravindran, P. Kasthuri, N. Marwan, J. Kurths, and R. Sujith, 2022: Study of interaction and complete merging of binary cyclones using complex networks. *arXiv preprint arXiv:2205.11789*.

Ditchek, S. D., J. Molinari, and D. Vollaro, 2017: Tropical cyclone outflow-layer structure and balanced response to eddy forcings. *Journal of the Atmospheric Sciences*, **74 (1)**, 133 – 149, https://doi.org/10.1175/JAS-D-16-0117.1.

Dong, K., and C. J. Neumann, 1983: On the relative motion of binary tropical cyclones. *Monthly Weather Review*, **111 (5)**, 945 – 953, https://doi.org/10.1175/1520-0493(1983)111⟨0945:OTRMOB⟩2.0.CO;2.

Doyle, J. D., and Coauthors, 2017: A view of tropical cyclones from above: The tropical cyclone intensity experiment. *Bulletin of the American Meteorological Society*, **98 (10)**, 2113 – 2134, https://doi.org/10.1175/BAMS-D-16-0055.1.

Dritschel, D. G., and D. W. Waugh, 1992: Quantification of the inelastic interaction of unequal vortices in two-dimensional vortex dynamics. *Physics of Fluids A: Fluid Dynamics*, **4 (8)**, 1737–1744, https://doi.org/10.1063/1.858394, https://doi.org/10.1063/1.858394.

Emanuel, K., 2012: Self-stratification of tropical cyclone outflow. Part II: Implications for storm intensification. *Journal of the Atmospheric Sciences*, **69 (3)**, 988 – 996, https://doi.org/10.1175/JAS-D-11-0177.1.

Falkovich, A. I., A. P. Khain, and I. Ginis, 1995: Motion and evolution of binary tropical cyclones in a coupled atmosphere–ocean numerical model. *Monthly Weather Review*, **123 (5)**, 1345 – 1363, https://doi.org/10.1175/1520-0493(1995)123⟨1345:MAEOBT⟩2.0.CO;2.

Fujiwhara, S., 1921: The natural tendency towards symmetry of motion and its application as a principle in meteorology. *Quarterly Journal of the Royal Meteorological Society*, **47 (200)**, 287–292, https://doi.org/https://doi.org/10.1002/qj.49704720010, https://rmets.onlinelibrary.wiley.com/doi/pdf/10.1002/qj.49704720010.

Fujiwhara, S., 1931: Short note on the behavior of two vortices. *Proceedings of the Physico-Mathematical Society of Japan. 3rd Series*, **13 (3)**, 106–110.

Komaromi, W. A., and J. D. Doyle, 2017: Tropical cyclone outflow and warm core structure as revealed by HS3 dropsonde data. *Monthly Weather Review*, **145 (4)**, 1339 – 1359, https://doi.org/10.1175/MWR-D-16-0172.1.

Lander, M. A., 1996: Specific tropical cyclone track types and unusual tropical cyclone motions associated with a reverse-oriented monsoon trough in the western north Pacific. *Weather and Forecasting*, **11 (2)**, 170 – 186, https://doi.org/10.1175/1520-0434(1996)011⟨0170:STCTTA⟩2.0.CO;2.

Lander, M. A., and G. J. Holland, 1993: On the interaction of tropical-cyclone-scale vortices. I: Observations. *Quarterly Journal of the Royal Meteorological Society*, **119 (514)**, 1347–1361, https://doi.org/https://doi.org/10.1002/qj.49711951406, https://rmets.onlinelibrary.wiley.com/doi/pdf/10.1002/qj.49711951406.

Liu, H.-Y., and Z.-M. Tan, 2016: A dynamical initialization scheme for binary tropical cyclones. *Monthly Weather Review*, **144 (12)**, 4787 – 4803, https://doi.org/10.1175/MWR-D-16-0176.1.

May, R. M., and Coauthors, 2022: Metpy: A Python package for meteorological data. Unidata, urlhttps://github.com/Unidata/MetPy, https://doi.org/10.5065/D6WW7G29.

Mehra, A., V. Tallapragada, Z. Zhang, B. Liu, L. Zhu, W. Wang, and H.-S. Kim, 2018: Advancing the state of the art in operational tropical cyclone forecasting at Ncep. *Tropical Cyclone Research and Review*, **7 (1)**, 51–56, https://doi.org/https://doi.org/10.6057/2018TCRR01.06.

Merill, R. T., 1988b: Environmental influences on hurricane intensification. *Journal of Atmospheric Sciences*, **45 (11)**, 1678 – 1687, https://doi.org/10.1175/1520-0469(1988)045⟨1678:EIOHI⟩2.0.CO;2.

Merrill, R. T., 1988a: Characteristics of the upper-tropospheric environmental flow around hurricanes. *Journal of Atmospheric Sciences*, **45 (11)**, 1665–1677.

Merrill, R. T., and C. S. Velden, 1996: A three-dimensional analysis of the outflow layer of Supertyphoon Flo (1990). *Monthly Weather Review*, **124 (1)**, 47 – 63, https://doi.org/10.1175/1520-0493(1996)124⟨0047:ATDAOT⟩2.0.CO;2.

Nguyen, L. T., J. Molinari, and D. Thomas, 2014: Evaluation of tropical cyclone center identification methods in numerical models. *Monthly Weather Review*, **142 (11)**, 4326 – 4339, https://doi.org/10.1175/MWR-D-14-00044.1.

Pasch, R. J., R. Berg, D. P. Roberts, and P. P. Papin, 2021: National Hurricane Center tropical cyclone report: Hurricane Laura. National Hurricane Center, URL https://www.nhc.noaa.gov/data/tcr/AL132020_Laura.pdf.

Prieto, R., B. D. McNoldy, S. R. Fulton, and W. H. Schubert, 2003: A classification of binary tropical cyclone–like vortex interactions. *Monthly Weather Review*, **131 (11)**, 2656 – 2666, https://doi.org/10.1175/1520-0493(2003)131⟨2656:ACOBTC⟩2.0.CO;2.

Rappin, E. D., M. C. Morgan, and G. J. Tripoli, 2011: The impact of outflow environment on tropical cyclone intensification and structure. *Journal of the Atmospheric Sciences*, **68 (2)**, 177 – 194, https://doi.org/10.1175/2009JAS2970.1.

Rolph, G., A. Stein, and B. Stunder, 2017: Real-time environmental applications and display system: Ready. *Environmental Modelling & Software*, **95**, 210–228.

Ryglicki, D. R., J. D. Doyle, D. Hodyss, J. H. Cossuth, Y. Jin, K. C. Viner, and J. M. Schmidt, 2019: The unexpected rapid intensification of tropical cyclones in moderate vertical wind shear. Part III: Outflow–environment interaction. *Monthly Weather Review*, **147 (8)**, 2919 – 2940, https://doi.org/10.1175/MWR-D-18-0370.1.

Shi, J.-J., S. W.-J. Chang, and S. Raman, 1990: A numerical study of the outflow layer of tropical cyclones. *Monthly Weather Review*, **118 (10)**, 2042 – 2055, https://doi.org/10.1175/1520-0493(1990)118⟨2042:ANSOTO⟩2.0.CO;2.

Stein, A., R. R. Draxler, G. D. Rolph, B. J. Stunder, M. Cohen, and F. Ngan, 2015: NOAA's HYSPLIT atmospheric transport and dispersion modeling system. *Bulletin of the American Meteorological Society*, **96 (12)**, 2059–2077.

Wu, C.-C., and K. A. Emanuel, 1994: On hurricane outflow structure. *Journal of the atmospheric sciences*, **51 (13)**, 1995–2003.